

Novel graphene-based nanostructures: physicochemical properties and applications

L A Chernozatonskii,^a P B Sorokin,^{a, b} A A Artukh^a

^a *N M Emanuel Institute of Biochemical Physics, Russian Academy of Sciences
ul. Kosygina 4, 119334 Moscow, Russian Federation*

^b *Technological Institute for Superhard and Novel Carbon Materials
ul. Tsentralnaya 7a, 142190 Moscow, Troitsk, Russian Federation*

The review concerns graphene-based nanostructures including graphene nanoribbons a few nanometres wide, structures functionalized with hydrogen and fluorine atoms as well as pure carbon composites. The physicochemical properties and the chemical engineering methods for their fabrication are considered. Methods for solving problems in modern nanotechnology are discussed. Possible applications of graphene and graphene-based nanostructures in various devices are outlined. The bibliography includes 286 references.

Contents

I. Introduction	251
II. Graphene nanoribbons	254
III. Functionalized graphene	258
IV. Graphene-based composites	268
V. Conclusion	273

I. Introduction

Graphene belongs to the most promising materials for nanotechnology in the 21st century. The properties of graphene, such as the electrical conductivity, mechanical strength and chemical stability underlie great prospects for application of the material in various devices as conductive nanoscale elements of high-frequency transistors, solar cells, sensors, supercapacitors and in various composites.

Graphene is a low-dimensional structure representing a one-atom thick graphite layer built of sp²-hybridized carbon atoms. Main electronic properties of graphene were correctly described in the pioneering study¹ using the tight-binding approximation (TBA) which takes into account only π -electrons from neighbouring atoms. This approach

was also employed in the first quantum chemical description of fullerene C₆₀ which can be considered as fragment of graphene sheet with twelve pentagonal topological defects. The electronic spectrum of C₆₀ calculated using the Hückel method² (in essence, also with inclusion of only nearest-neighbour interactions) was only slightly different from the experimental spectrum and from the results of more precise calculations.³

Pioneering studies on quasi-two-dimensional (2D) materials including graphene were carried out by a research group which included winners of the 2010 Nobel prize in physics A K Geim and K S Novoselov. However, it should be noted that long before these investigations were performed, fabrication of films with thickness from a few tens^{4–6} to a few⁷ graphene monolayers was reported. However, researchers from the group mentioned above succeeded not only in fabricating an individual graphene sheet, but also discovered and thoroughly studied its physical and chemical properties.⁸ A comprehensive study on the prehistory of graphene can be found in Geim's paper.⁹

The discovery of graphene opened a new field in chemistry, namely, chemistry of 2D materials. The scope of the new field includes, in particular, research on functionalized graphene (graphene sheets bearing functional groups),¹⁰ which is of interest for electronics, optics, as well as for the design of composite materials¹¹ and catalysts.¹² The synthesis of monolayer, multilayer and modified graphene structures^{13, 14} has been a subject of about ten reviews (see, *e.g.*, Ref. 15 and references cited therein). The

L A Chernozatonskii Doctor of Physical and Mathematical Sciences, chief researcher of the IBCP RAS. Tel. (7-495) 939 71 72, e-mail: cherno@sky.chph.ras.ru

P B Sorokin Candidate of Physical and Mathematical Sciences, senior researcher of the TISNCM. Tel. (7-499) 272 23 14, e-mail: PBSorokin@gmail.com

A A Artukh Graduate student of the IBCP RAS. Tel. (7-495) 939 71 72, e-mail: anastasiia2000@mail.ru

Current research interests: condensed matter physics, nanomaterials, computer modelling.

Received 29 December 2012

Uspekhi Khimii 83 (3) 251–279 (2014); translated by A M Raevskiy

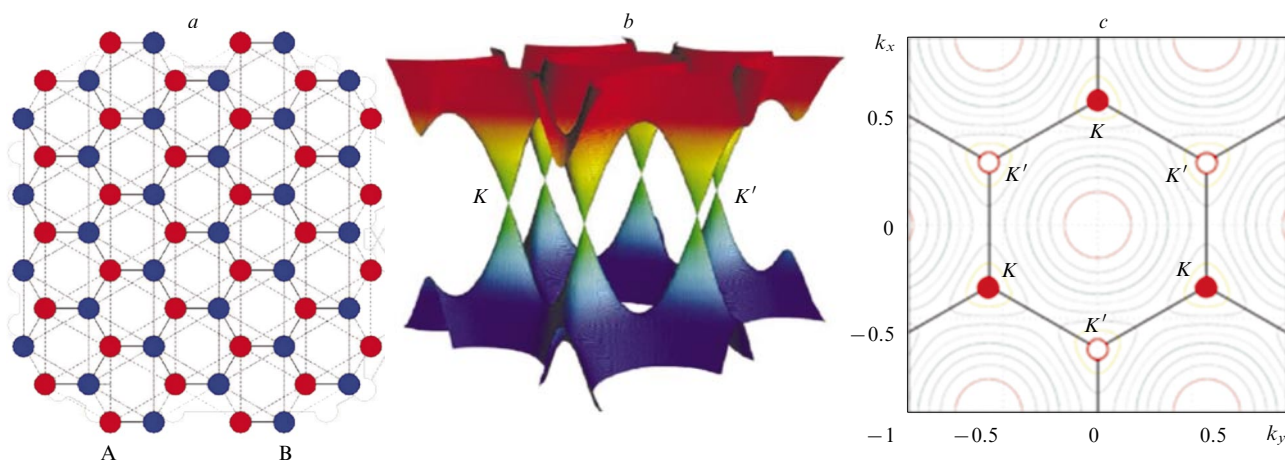


Figure 1. Graphene lattice with two equivalent sublattices A and B (a), energy bands with two nonequivalent Dirac cones K and K' (b) and isoenergy lines $E(k_x, k_y) = \text{const}$ (c).¹ (c) The hexagon represents the first Brillouin zone; also, shown are the regions at the corners of the first Brillouin zone where charge carriers have linear dispersion relations.

available information on methods for modification of graphene-based carbon materials through creation of structural defects by introducing impurities, adsorption of alien atoms, mechanical deformations, as well as the structure, properties and results of simulation of graphene derivatives and related non-carbon graphene-like materials (structural analogues of graphene) is generalized in a recent study.¹⁶

The structure of graphene is not a simple Bravais lattice. Its unit cell contains two carbon atoms (Fig. 1a). Since electrons and holes are fermions, in the TBA model of graphene they are described by a Dirac-like equation for zero-mass particles and antiparticles by analogy to the equation for massless neutrino; therefore, the convergence points, K and K' (Fig. 1b), of the cones are called the Dirac points.^{17,18} Electrons in graphene near the Fermi level passing through these points have a linear dispersion relation, like photons, but their effective velocity is 300 times lower than the velocity of light

$$v_F \approx \frac{c}{300}$$

Regions near the convergence points K and K' at the corners of the Brillouin zone (Dirac cones) represent two valleys in the k -space with nonequivalent wave vectors (\mathbf{k}), where the dispersion relation for charge carriers is linear (see Fig. 1b,c):

$$E(\mathbf{k}) = \pm v_F |\mathbf{k}|, v_F \approx 10^6 \text{ m s}^{-1}$$

Dirac cones are rather stable against mechanical deformations of graphene; they do not disappear even upon appearance of elastic corrugations (~ 0.5 nm in height with ~ 5 nm separations) due to nonlinear elastic properties on a freely suspended graphene sheet.¹⁹

Such a ‘quantum electrodynamic’ character of the graphene spectrum leads to a specific tunnelling of charge carriers that is known as the Klein paradox.²⁰ This phenomenon is related to a nontrivial behaviour of the transmittance of relativistic particles in the case of potential barriers that are higher than twice the rest energy of the

particle. There exists an analogue of the Klein paradox for particles in graphene except that an electron has zero effective mass. Such an electron propagates through all kinds of potential barriers with a 100% probability provided normal incidence on the interface. In other cases, the electron reflection probability differs from zero and depends on the angle of incidence. For instance, a conventional p–n junction appears to be a penetrable barrier in graphene.²¹ By and large, the Klein paradox leads to difficulties in locating particles in graphene, which in turn means that the particles have high mobilities. The Klein paradox leads to tunnelling of charge carriers from the K region to the K' region in the k -space even in the case of random scattering potential;²² actually, it leads to the notion of quantum resistance. This conductivity type bears no relation to Bloch waves in conventional conductive crystals. Taking into account ‘ballistic’ character of the motion of charge carriers in graphene made it possible to design novel efficient devices.^{23–27}

If an electrical voltage V_g is applied normal to the surface of a graphene sheet (Fig. 2a: the potential difference between graphene and silicon substrate separated by a SiO_2 dielectric layer), the chemical potential — the Fermi level in the spectrum — is shifted (at $V_g < 0$, it lies above the Dirac point; at $V_g > 0$, it lies below the Dirac point). In other words, one deals with a specific kind of doping, namely, graphene becomes an electron or hole conductor at negative or positive V_g values, respectively (Fig. 2b). The concentration of charge carriers (N) can be varied by varying the voltage V_g that is simply related to N

$$N (\text{cm}^{-2}) = 7.2 \times 10^{14} V_g$$

provided a SiO_2 thickness of 300 nm.

The problem of high finite resistance R that is inversely proportional to N at $V_g = 0$ and at subzero temperatures (see Fig. 2b,c) was solved in theoretical studies (see review¹); however, its consideration goes beyond the scope of this publication.

The effective mass of charge carriers depends on the square root of concentration:²⁴

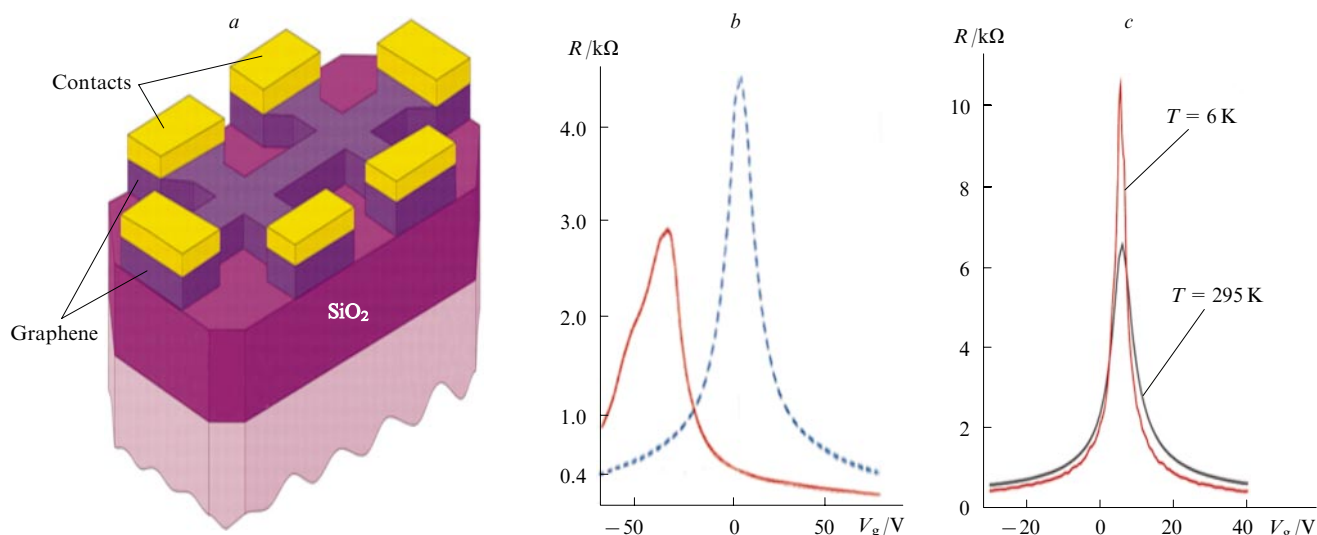


Figure 2. A schematic (a) and results of experimental measurement of electrical resistance (R) (b, c). (a) Graphene on SiO_2 substrate; shown are contacts (gate voltage V_g is applied to a contact and n-type conductive silicon substrate);²⁶ data for graphene field-effect transistors are plotted vs. V_g for doped graphene with n-type conductivity (b)²⁷ and p-type conductivity (c);²⁵ dashed line denotes the results of measurements for undoped graphene (Scheme a).

$$m_c = \sqrt{\frac{\hbar^2 N}{4\pi v_F^2}}$$

Doping graphene with certain atoms in polyvinyl alcohol leads to the onset of n-type conductivity and to shift of the $R(V_g)$ curve towards negative voltages (see Fig. 2b), while doping in concentrated nitric acid causes the onset of p-type conductivity and a shift of the $R(V_g)$ curve towards positive voltages (see Fig. 2c).²⁵

In spite of considerable progress in the design of silicon chips in the last decade, silicon-based technologies approach their limits.²⁸ Predictions were made that fabrication of 10-nm transistors will be started by 2018. This will require a 10-nm linear resolution of lithographic equipment. Taking into account this fact, the development of alternative methods free from drawbacks intrinsic in silicon technologies becomes of particular importance. The main drawback of the silicon technologies is the impossibility of further miniaturization owing to high defectiveness of silicon nanocrystals.

Graphene seems to be the best candidate for the design of various devices because it has high thermal conductivity and very high charge carrier mobility ($10^6 \text{ cm}^2 \text{ V}^{-1} \text{ s}^{-1}$ for suspended graphene and $10^4 \text{ cm}^2 \text{ V}^{-1} \text{ s}^{-1}$ for supported graphene).²³ However, methods for large-scale production of devices involving exact positioning of graphene components on a solid substrate are unavailable. Also, the design of high-performance integrated devices requires combining graphene with high-dielectric-constant materials as well as controlling the charge carrier concentration in graphene layers. To date, operation of a 155-GHz graphene transistor was demonstrated.²⁹ One can hope for successful fabrication of terahertz-frequency transistors based on nearly 10-nm wide graphene nanoribbons. Clearly, new nanotechnologies involving chemical lithography processes and technologies for template growth of graphene nanoribbons will enable production of chips for, e.g., mobile communication

devices and small computers with much lower energy consumption.[†]

Graphene exhibits interesting optical properties. Theoretically, the transmittance (η) of freestanding graphene is:³¹

$$\eta = (1 + 0.5\pi\alpha) - 2 \approx 1 - \pi\alpha \approx 97.7\%$$

where

$$\alpha = \frac{e^2}{\hbar c} = \frac{1}{137}$$

is the fine structure constant, e is the charge of electron, \hbar is the Planck constant and c is the velocity of light *in vacuo*.

Light absorption by a graphene sheet occurs uniformly, starting with the long-wavelength region (this is typical of 2D materials). In the UV region, the absorption spectrum exhibits a peak at about 250 nm corresponding to interband electronic transitions.³² The transmittance values (Fig. 3) of mechanically cleaved graphene (97.7%)³³ and high-quality graphene synthesized by chemical vapour phase deposition (97.4%)²⁵ are very close to the theoretical value.

Optical absorption is a linear function of the number of graphene layers, each layer being characterized by an absorbance of 2.3% in the visible region (see Fig. 3a). A multilayer specimen can be treated as weakly interacting, optically equivalent layers of 2D electron gas.³⁴

Novel transparent graphene electrodes on flexible substrates can be utilized in optoelectronic devices. They have a record low resistance per unit surface area ($\sim 20 \Omega$).³⁵ Unlike their analogues, ITO electrodes (ITO is tin-doped indium oxide), the conducting properties of the graphene

[†] Technologies for fabrication of large graphene transistor arrays have been developed for 2–3 years by a research group headed by Professor W A de Heer (Georgia Institute of Technology, Atlanta, GA, USA). Recently, they reported fabrication of graphene transistor arrays with a density of 4×10^4 per cm^2 on a silicon carbide substrate.³⁰

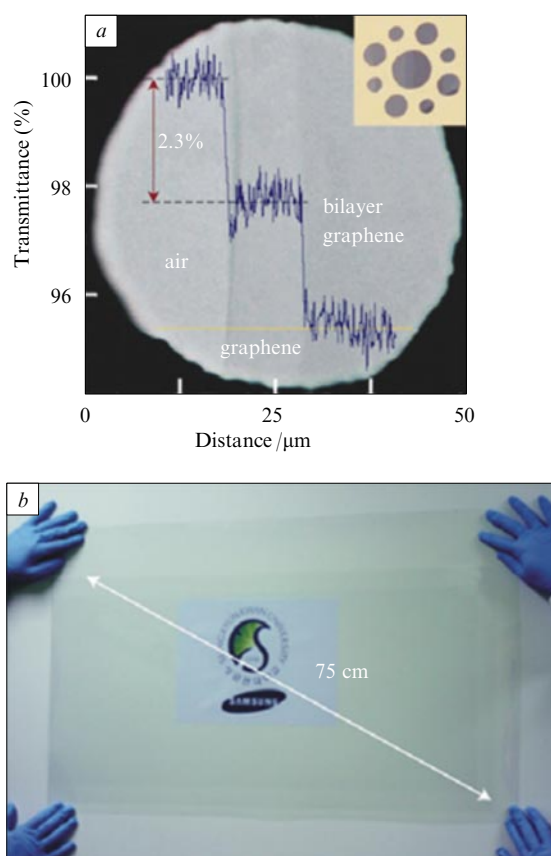


Figure 3. Light transmission by mechanically cleaved graphene sheet (a) (inset: photograph of an orifice in the substrate covered with graphene)³³ and a photograph of a graphene film with a sheet resistance of about 125 Ω and a transmittance of $\sim 97.7\%$ grown by chemical vapour phase deposition from a poly(ethylene terephthalate) layer on substrate (b).²⁵

electrodes do not deteriorate upon multiple large deformations. For instance, graphene electrodes are promising for application in solar cells,³⁶ photodetectors³⁷ and transistors,²⁹ where high conductivity of electrodes is required to maintain efficient transport of charge carriers.

Graphene is electrochemically stable material and can be used as anode or cathode in electrochemical light-emitting cells, analogues of polymeric light-emitting diodes. Non-metallic light-emitting elements with carbon electrodes are good candidates for the design of devices with operating surface areas of the order of a few square centimetres.³⁵ The enhancement of photocurrent attained using plasmon resonance on gold and titanium nanoclusters placed on graphene near contacts was an order of magnitude higher compared to pure graphene.³⁸ This technology is expected to find applications in high-speed optical devices.

A new family of efficient, graphene-based static electric charge integrators for fabrication of supercapacitor plates was reported.³⁹ Here, the number of capacitor plates can be very large while the distances between differently charged plates are on the nanometre scale. The advantage of supercapacitors consists in high charge–discharge rate and high energy density; therefore, they potentially can store electricity much more efficiently than conventional capacitors do. Modern graphene-based supercapacitors store almost

the same charge per unit mass as the best commercially available capacitors and theoretical limits are far from being approached.³⁹ Indeed, graphene has high internal conductivity, thermal stability, it is chemically inert and thus appropriate for being used in supercapacitors. For instance, graphene-based capacitors fabricated and reported by Kaner and co-workers⁴⁰ are characterized by much higher charge–discharge rates than conventional storage cells, although they store the same amount of energy. However, application of graphene in supercapacitors faces some difficulties; in particular, the irreversible capacitance in the graphene-based capacitors is inappropriately high, probably, due to the defect structure of the material.⁴¹

In spite of nanometre-scale thickness, graphene exhibits unique mechanical properties, namely, its strength and flexibility are higher than those of steel.⁴² These properties open prospects for the design of novel mechanical devices based on graphene including membranes, vibratory sources, flexible touch screens, *etc.*

Detailed reviews on the fabrication and chemical modification of graphene with various compounds were reported by Grayfer *et al.*¹³ and by Wei and Liu.⁴³ In this review, we will briefly outline the amazing physical properties of graphene (‘CERN on the desk’¹⁷ according to well-known theoretical physicist M I Katsnelson[‡]), consider problems that were little covered earlier and then analyze the results of studies that were left out of consideration by the authors of the previous reviews. The case in point is research on the physicochemical properties of GNRs, functionalized graphene and graphene–carbon nanotube (CNT) composites. These types of nanostructures are likely to have applications in new-generation devices and future materials and therefore attract the attention of many researchers.

II. Graphene nanoribbons

The invention of graphene was followed by the rise of interest in GNRs. One can assume that it is just the structures fabricated from GNRs a few nanometres wide that will become key elements for nanoelectronics, playing the role of nanodiodes and nanotransistors, and elements for spintronics devices. Recently, there has been considerable progress in the technology of fabrication of GNRs.¹⁵ Usually, GNRs have ‘zigzag’ and ‘armchair’ edges. In the former case, two C–C bonds in each hexagon are perpendicular to the GNR axis. In the latter case, these bonds are aligned with the GNR axis. The properties of GNRs terminated with different-type edges were investigated in the early TBA studies.^{44,45} For instance, it was predicted that ‘armchair’ GNRs should exhibit the properties of semiconductors whose band gaps oscillate depending on the GNR width. Graphene nanoribbons with the number, n , of the edge carbon atoms equal to $3p + 1$ (p is a positive integer) have wider band gaps than the GNRs with $n = 3p$ and $n = 3p + 2$. The TBA studies^{44,45} cited above were performed without atomic structure optimization and pre-

[‡] M I Katsnelson is a theoretical physicist, Professor at the Radboud University Nijmegen (The Netherlands). Since 2004, he collaborates with the research group of A K Geim and K S Novoselov at the Manchester University (United Kingdom). In 2013, M I Katsnelson was awarded the Spinoza Prize (highest scientific award in the Netherlands) for application of concepts of physics of elementary particles to research on graphene.

dicted that ‘armchair’ GNRs with $n = 3p + 2$ should behave as semimetals. However, more recent calculations^{46–48} using more exact *ab initio* quantum chemical methods revealed a semiconductor character of this subtype of GNRs. Band gap oscillations upon changes in the GNR width are directly related to size quantization in semimetallic graphene; they are observed in many graphene-based nanostructures (CNTs,⁴⁹ graphene bearing ‘lines’ of adsorbed hydrogen atoms⁵⁰ and graphene nanoroads in graphene⁵¹ and fluorographene⁵²).

‘Zigzag’ GNRs should exhibit the properties of antiferromagnets,^{47,53,54} have band gaps < 0.1 eV and their band gaps should monotonically decrease as the GNR width increases.⁴⁸ The spin density on the ‘zigzag’ GNRs and on all other graphene fragments with ‘zigzag’ edges should mainly concentrate at the edges. This was confirmed experimentally,⁵⁵ namely, a localized spin state was observed on the ‘zigzag’ edge of a graphene fragment.

The possibility for ‘zigzag’ GNRs to exhibit the properties of semiconductors was debated. In particular, it was found that the electronic structure of the ‘zigzag’ GNRs is sensitive to the type of the edge-terminating atoms and to the edge reconstruction method.^{56–58} Also, the edge of a ‘zigzag’ GNR is energetically not too stable and can be reconstructed, with the loss of magnetic properties, to a so-called ‘reczag’-type edge with alternating pentagons and heptagons. The energy difference between the ‘zigzag’ and ‘reczag’ edges is $0.35 \text{ eV } \text{Å}^{-1}$ (see Ref. 58). Partial ‘zigzag’-to-‘reczag’ edge reconstruction was reported.⁵⁹ Mention was also made^{60,61} that such a reconstruction is energetically favourable only for freestanding graphene, because for metal surfaces, the ‘zigzag’ edge is energetically more preferable. Thus, the atomic structure and properties of ‘zigzag’ GNRs remain unknown and more precise experiments are required to address these points.

To date, experimental studies revealed a clearly seen dependence of the band gap of the ‘reczag’ GNRs on the GNR width. Figure 4 presents theoretical estimates obtained from the density functional calculations;⁴⁶ these values are the closest to the experimental data. As can be seen, GNRs exhibit the properties of semiconductors only to a width of about 10 nm; this remains the key obstacle to application of GNRs in electronics.

Now we will dwell on methods for the synthesis of GNRs with widths up to 10 nm. The first procedure for fabrication of narrow GNRs⁶² allows one to synthesize ribbons with smooth edges. In the experiment, graphite was exfoliated upon rapid (60 s) heating to 1000 °C in a hydrogen (3%)/argon (97%) mixture. The exfoliated graphite was dispersed in a solution of poly(*m*-phenylenevinylene-*co*-2,5-diethoxy-*p*-phenylenevinylene) (PmPV) in 1,2-dichloroethane under sonication (30 min) to give a homogeneous suspension. Large particles were removed by centrifugation. Among other particles, an inspection by atomic force microscopy revealed GNRs with widths from 1 to 10 nm; their band gaps corresponded to item 1 in Fig. 4. The main drawback of this procedure consists in complexity of control of the shape of the GNR edges, which to a great extent determine the electronic properties of GNRs (see above). Also, since GNRs are assumed to be used as elements for electronic circuits, it is desired to fabricate them from ready-made units.

From this standpoint, cutting of graphene sheets into ribbons seems to be promising. In particular, this was done

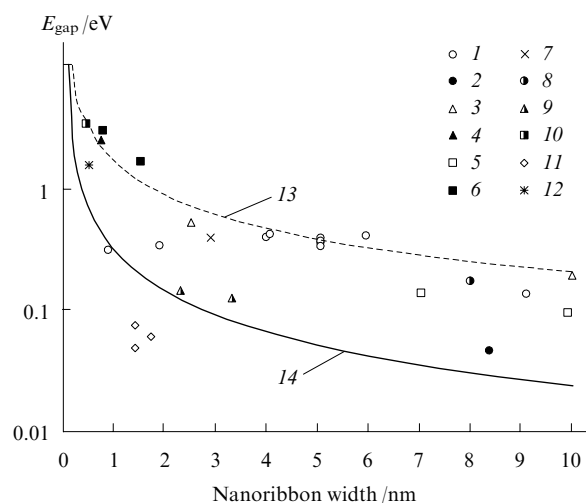


Figure 4. Averaged experimental values (symbols 1–12) and theoretical band gap (E_{gap}) estimates (solid lines) for up to 10 nm wide graphene nanoribbons.

Data were taken from Refs 62 (1), 63 (2), 64 (3), 65 (4, ‘armchair’ nanoribbon edges), 66 (5), 67 (6, ‘armchair’ nanoribbon edges), 55 (7, ‘armchair’ nanoribbon edges), 68 (8), 55 (9, ‘zigzag’ nanoribbon edges), 69 (10), 70 (11), 71 (12), 46 (13, $3p + 1$), and 46 (14, $3p + 2$).

using a scanning tunneling microscope with high potential difference between the microscope tip and graphene.⁶⁴ Graphene is cut as a result of the interaction with the ‘sharp’ electron beam emitted from the tip. The resultant ‘armchair’ GNRs with a width of 2.5 nm and perfect (defect-free) structure are shown in Fig. 4 (item 3). Graphene ribbons less than 1-nm wide were fabricated with a focused electron beam.⁷²

Arrays of GNRs with nanometre-scale widths were fabricated by etching of graphene protected with a block copolymer film.^{73,74} Fabrication of graphene nanomeshes by nanoimprint lithography was reported.^{65,66} The graphene system can be treated as an array of interconnected GNRs. Graphene specimens covered with a block copolymer film⁷⁵ and polystyrene film⁶⁶ with hexagonally patterned orifices were treated with oxygen plasma to form hexagonal networks of GNRs with widths from 7 to 20 nm (see Fig. 4, item 5). Also, wide (20–30 nm) GNRs fabricated by electron-beam lithography were etched.⁷⁶ This technique makes it possible to obtain both conventional and multiterminal GNRs (analogues of multiterminal CNTs) with widths < 10 nm.

A promising method for fabrication of GNRs is to use other quasi-1D materials with nanometre-scale crosswise size.⁷⁶ For instance, silicon wires with nanometre-scale diameters aligned on graphene specimens were used.⁶⁸ The wires protected the graphene from the action of oxygen plasma and made it possible to obtain GNRs with widths from 6 nm. Carbon nanotubes were also cut into ribbons. The surface of CNTs was etched using nickel and cobalt clusters⁷⁷ at 850 °C in $\text{H}_2 + \text{Ar}$ gas atmosphere to obtain CNTs that were both completely and partially cut along the axis.

Multi-walled CNTs can be converted to GNR ‘stacks’ by heating to 1800 °C.⁷⁸ A similar transformation occurs upon annealing of multi-walled CNTs at high pressure (5.5 GPa)⁷⁹ and on intercalation of multi-walled CNTs

with lithium followed by exfoliation at 1000 K.⁸⁰ Also, CNTs were longitudinally cut in the oxidation with potassium permanganate in the presence of concentrated sulfuric acid.⁸¹ This technique appeared to be highly efficient, namely, the yield of GNRs was nearly 100%, but the GNRs were of low quality owing to defectiveness. In another study reported by the same research group,⁸² CNTs were cut upon oxidation at 60 °C in the presence of KMnO_4 as oxidant and concentrated H_2SO_4 (or trifluoroacetic acid and H_3PO_4). Graphene nanoribbons thus fabricated had high-quality atomic structures and good conductivities. More recently, a method for fabrication of GNRs by the action of potassium vapours on CNTs was developed.⁸³ Hydrogenation of CNTs also gives GNRs.⁸⁴ It was shown that hydrogenation at 400–550 °C leads to opening of CNTs and formation of hydrogen-terminated GNRs. Yet another method⁸⁵ involves the oxidation of CNTs in a solution of PmPV in 1,2-dichloroethane. Oxygen reacted with pre-existing defects on CNTs to form etch pits on the CNT sidewalls. In the solution-phase sonication step, the pits enlarged and the structure unzipped into very narrow (about 1-nm wide) GNRs with almost same-type edges⁷⁰ and band gaps of 0.6–0.9 eV (see Fig. 4, item 11). This method was also used by Tao *et al.*,⁶³ who determined with high accuracy the type of the GNRs with widths from 8 to 20 nm. The GNR indexes were determined and the band gaps were measured (see Fig. 4, item 2).

A feature of one more physicochemical method for conversion of CNTs to GNRs^{86,87} consists in etching an axially unzipped CNT protected with a poly(methyl methacrylate) (PMMA) film in argon plasma (Fig. 5a). The formation of single- or multilayer GNRs is governed by the etching time. By moving the AFM tip one can produce GNR junctions (see Fig. 5b).⁸⁷

The synthesis of GNRs by self-assembly is widely used. The technique is based on the well-known ‘bottom-up’ approach to the synthesis of nanostructures, where the desired nanostructures are assembled from smaller fragments. Cai *et al.*⁸⁸ were the first who employed this method to assemble ‘armchair’ GNRs with $n = 7$ from 10,10'-dibromo-9,9'-bianthryl (**1**) monomers (Scheme 1). In step 1, monomers deposited onto the Ag(111) surface by sublimation lost the halogen substituents; subsequent heat treatment caused surface diffusion of radicals that added to one another to form a linear polymer chain (**2**) (Fig. 6a). Then, an additional heat treatment was performed to cyclodehydrogenate the polymer and form ultranarrow GNRs (**3**) with $n = 7$ and perfect ‘armchair’ edges (Fig. 6b).

The structure and shape of the synthesized GNRs appeared to depend strongly on the type of the precursor molecules. For instance, the use of 6,11-dibromo-1,2,3,4-tetraphenyltriphenylene and 1,3,5-tris(4-iodo-2-biphenyl)-

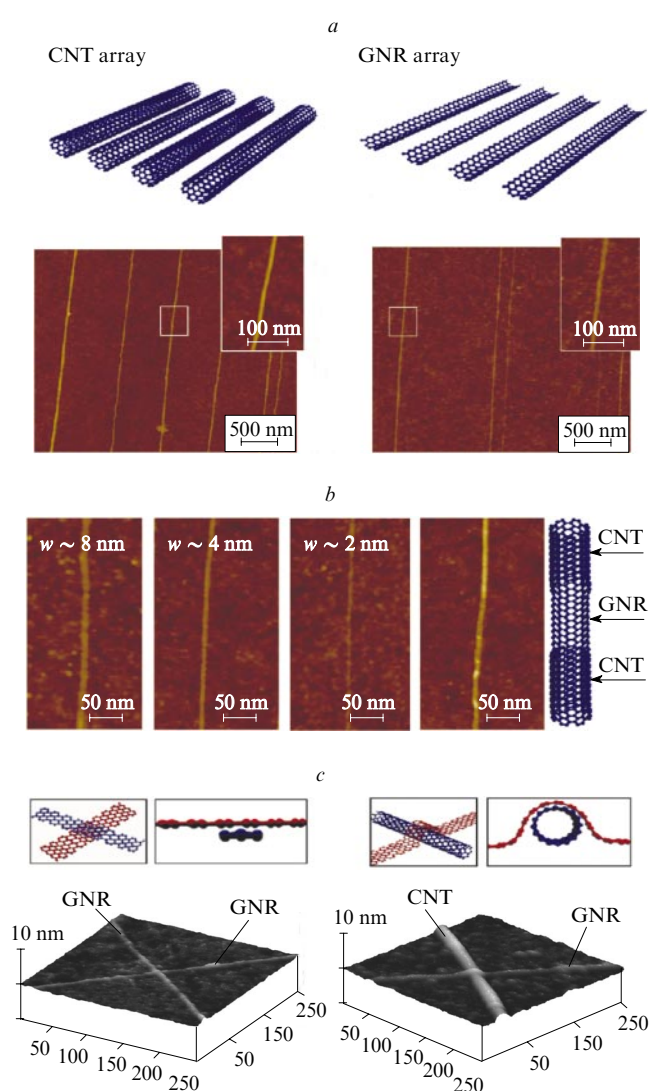
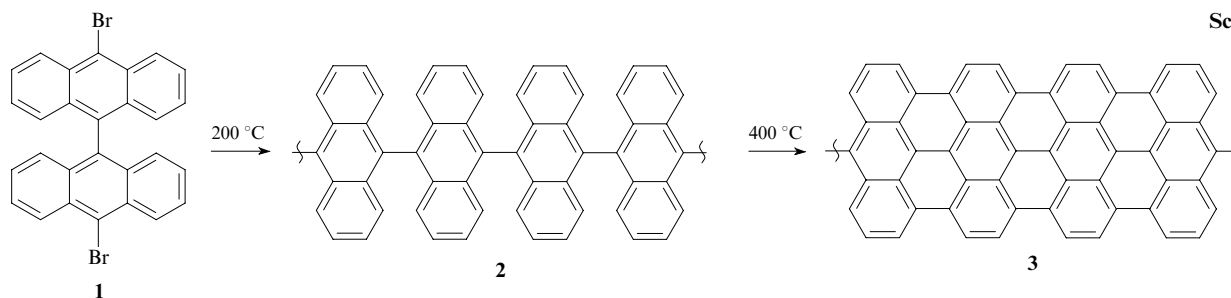


Figure 5. CNT arrays partially protected with a PMMA film, graphene nanoribbon (GNR) arrays and their AFM images (a), AFM images of individual GNRs of width 8, 4 and 2 nm and a hybrid structure called CNT–GNR junction and a schematic of CNT–GNR junctions and their AFM images (c). All AFM images were taken from Ref. 87; w is the nanoribbon width.

benzene instead of 10,10'-dibromo-9,9'-bianthryl respectively led to a chevron-type structure formed by ‘armchair’ GNRs with $n = 5$ (see Fig. 6c) and to an Y-shaped structure shown in Fig. 6d.



Scheme 1

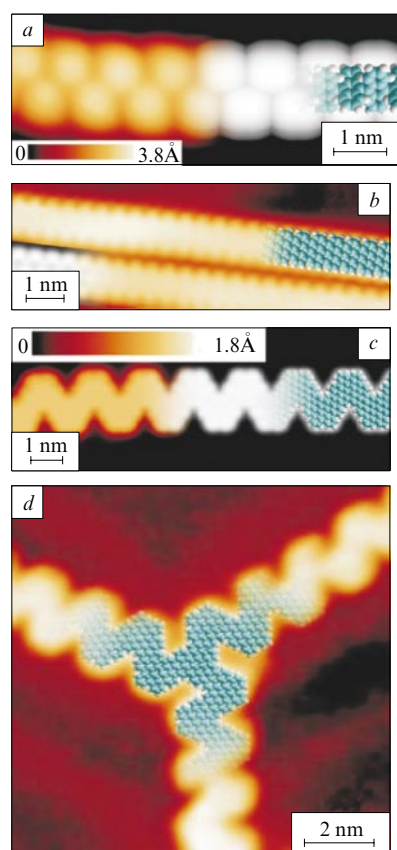
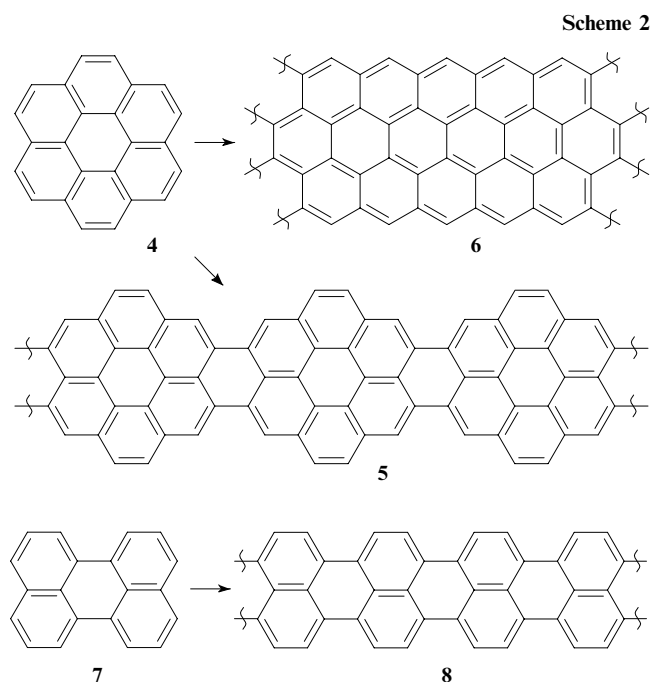


Figure 6. Linear polymer chain **2** (a) and graphene nanoribbon **3** (b) fabricated using Scheme 1 upon completion of steps 1 and 2, respectively; a chevron-type graphene nanoribbon obtained from 6,11-dibromo-1,2,3,4-tetraphenyltriphenylene using Scheme 1 (c) and Y-shaped structure (threefold junction) fabricated from chevron-type graphene nanoribbons resulting from the reaction between 6,11-dibromo-1,2,3,4-tetraphenyltriphenylene and 1,3,5-tris(4-iodo-2-biphenyl)benzene (d). All images are STM images; atomic models (see insets) were optimized within the framework of the density functional theory.⁸⁸

The method proposed by Cai *et al.*⁸⁸ was used in some other studies. In particular, the electronic structure of the GNRs fabricated by Cai *et al.*⁸⁸ was studied.⁶⁵ The energy band structure of the ‘armchair’ GNRs ($n = 7$) and the band gap width (see Fig. 4, item 4) were determined by photo-emission spectroscopy. Graphene nanoribbons with $n = 7$ and 13 were fabricated⁶⁷ following Cai *et al.*⁸⁸ and their electronic structure was studied (for the band gaps of the GNRs, see Fig. 4, item 6). The band gap width of the GNRs with $n = 7$ appeared to be somewhat larger than that reported by Ruffieux *et al.*⁶⁵

The ‘bottom-up’ strategy of synthesis was implemented in yet another study⁸⁹ with coronene and perylene as sources of carbon. The precursors were encapsulated into a single-walled CNT that played the role of a guide to limit molecular motion. After heat treatment at 350–450 °C, coronene (**4**) converted to a linear polymer **5** and ‘zigzag’ GNRs ($n = 4$) **6**. Perylene (**7**) converted to a narrow ‘armchair’ GNR ($n = 5$) **8** (Scheme 2).

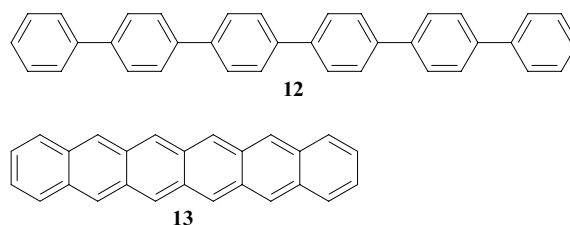
‘Zigzag’ GNRs ($n = 4$) formed from various organo-sulfur compounds encapsulated into a single-walled CNT



were reported.⁹⁰ In particular, fullerenes functionalized with organosulfur groups (**9**) (Fig. 7a) were encapsulated into the CNT (Fig. 7b). Under the action of an electron beam, they polymerized to give a GNR (see Fig. 7c). A comparison of experimental data (see Fig. 7d) and results of model calculations showed that the GNRs have ‘zigzag’ edges ($n = 4$) (see Fig. 7e). The presence of sulfur atoms makes the GNRs energetically more favourable structures compared to the starting materials. Therefore, sulfur atoms play a key role in the synthesis of GNRs. Graphene nanoribbons were also synthesized from some other organosulfur compounds. For instance, tetrathiafulvalene (**10**) and its mixture with fullerene (**11**) encapsulated into a CNT underwent polymerization to GNR under heat treatment or under the action of an electron beam.

It should be noted that thin, one-benzene-ring wide GNRs were synthesized and studied as long as five decades ago. These are hexaphenyl (**12**)⁹¹ and hexacene (**13**)⁹² with ‘armchair’ and ‘zigzag’ edges, respectively (see also review⁹³). Also, polyperinaphthalene (**8**) was synthesized in 1986.⁹⁴ Structurally, compound **8** is an ‘armchair’ GNR ($n = 5$).

Structures 12, 13



Summing up, rather efficient chemical methods for fabrication of GNRs with nanometre-scale widths have been developed to date. In the future, these methods may become a basis for large-scale production of such GNRs. Would a method for controlling the structure of the GNR edges be available, one can expect that this nanomaterial

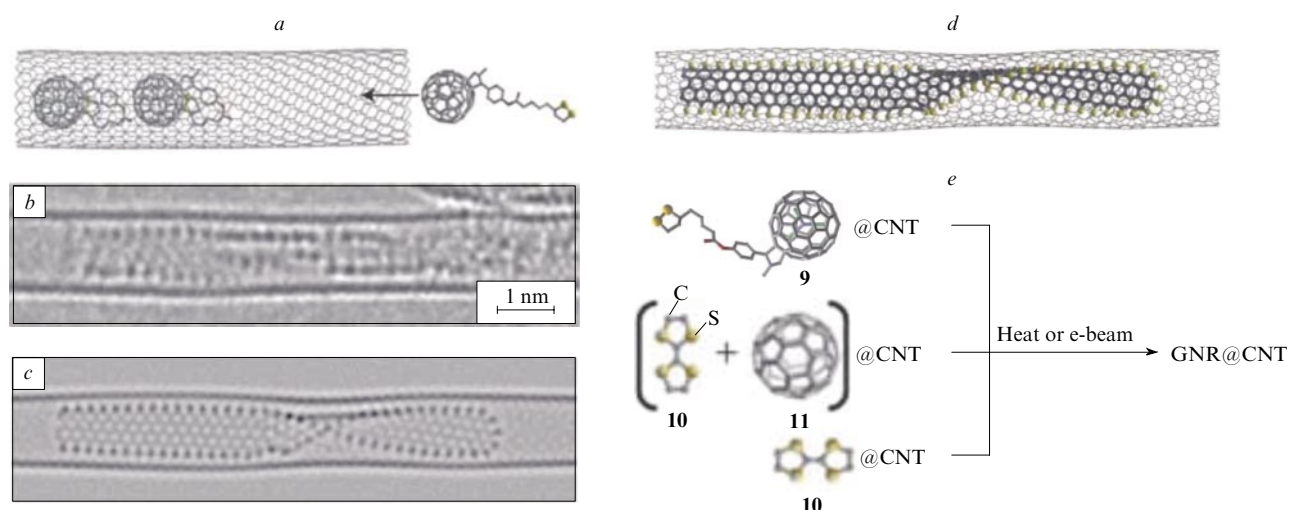


Figure 7. Results of functionalization of single-walled CNTs with sulfur-containing organic compounds.⁹⁰ Functionalized fullerenes **9** bearing organic groups with sulfur atoms are encapsulated into a single-walled CNT (*a*); under exposure to electron beam, fullerenes re-assemble into graphene nanoribbons with sulfur-passivated edges (dark-grey spots in the image) (*b*). This is confirmed by a model image (*c*) simulated from the atomic structure of the nanoribbon (*d*). Graphene nanoribbons with sulfur-passivated edges can be formed from other sulfur-containing organic molecules such as tetrathiafulvalene (**10**) or its mixture with fullerene (**11**) inserted into nanotubes at 1000 °C or under electron beam radiation (*e*).

will find wide application in nanoelectronics as elements for semiconductor devices.

III. Functionalized graphene

Pristine graphene is of considerable interest as high-strength membrane or as highly efficient gas sensor.^{18,23} Graphene with the chemically modified surface can be used in semiconductor electronics¹⁵ as basis for organic light-emitting diodes,⁹⁵ biosensors,⁹⁶ supercapacitors, organic electrodes and polymer nanocomposites.⁹⁷

Graphene is a chemically inert material representing an infinite network of carbon atoms bonded by strong σ -bonds involving p_x - and p_y -orbitals; p_z -orbitals form a unified π -system. To adsorb atoms onto the surface, the graphene π -system should be broken down or locally distorted. At the same time, the graphene π -system participates in the formation of complexes with, *e.g.*, organic compounds and transition metals. The associated antibonding π^* molecular orbital facilitates adsorption of electron-rich particles, *e.g.*, alkali metals.⁹⁸

Atoms can be adsorbed onto graphene edges (Fig. 8*a*) with relative ease; this significantly affects only the properties of graphene nanoclusters or GNRs with nanometre-scale widths. To change the electronic structure, functionalization of graphene surface is required. This can be facilitated by lattice defects (either formed during the synthesis or intercalated into the synthesized structure) that can form chemical bonds with the adatoms (Fig. 8*b*). Also, structural distortions in bent graphene enhance the reactivity of its surface (Fig. 8*c*). In particular, theoretical studies of CNTs predicted^{99,100} that the probability of hydrogen chemisorption onto graphene surface is proportional to the local curvature of the graphene surface. This was confirmed experimentally.¹⁰¹ The reason is that bending of a graphene sheet causes the separation between p_z -orbitals to increase and the graphene π -system to loose.

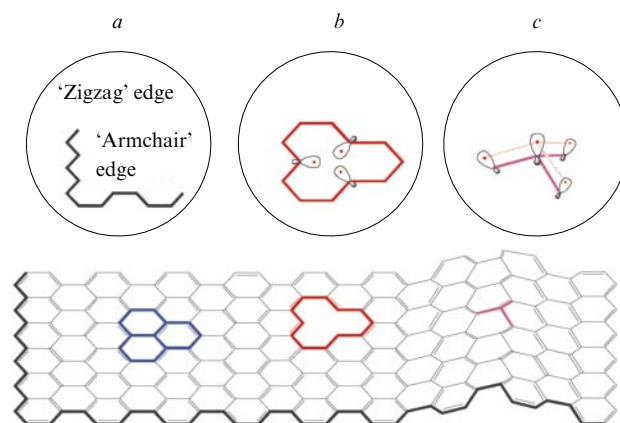


Figure 8. Reactive regions in graphene: edge (*a*), lattice defect (*b*), mechanically distorted structure (*c*).⁹⁸

Graphene can be functionalized with various atomic groups. In this review, we restricted ourselves to consideration of the best studied methods for chemical functionalization including hydrogenation, fluorination and oxidation. We will also present recent results on graphene doping with boron and nitrogen and on the formation of hexagonal boron nitride (h-BN) in the graphene structure.

1. Hydrogenated graphene

Prior to fabrication of free-standing graphene, a number of ground-state conformers of hydrogenated graphene was predicted,¹⁰² the ‘armchair’ conformer being the most energetically favourable. Fabrication of free-standing graphene was followed by sharp increase in interest in its functionalization. The properties of two most energetically favourable structures, ‘armchair’ and ‘boat’, were studied in detail by Sofo *et al.*,¹⁰³ who introduced the term ‘graphane’

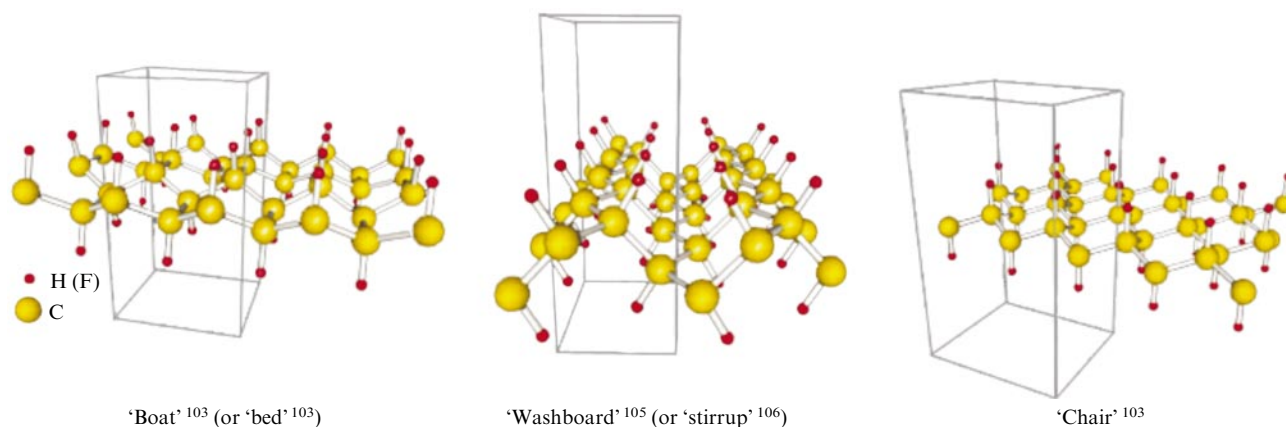


Figure 9. Atomic structures of energetically favourable conformers of hydrogenated (fluorinated) graphene.

for hydrogenated graphene; this term became a common word. The stability and electronic properties of graphane were investigated and, in particular, it was shown that full hydrogenation of graphene leads to the opening of a wide band gap ranging from 3.4 (see Ref. 103) to 6.1 eV (see Ref. 104). In other words, semimetallic graphene is transformed to dielectric graphane. The structures of the energetically favourable conformers of hydrogenated (fluorinated) graphene are shown in Fig. 9.

Subsequent experiments^{107,108} on hydrogenation of graphene appeared to be successful and by and large confirmed theoretical predictions. Hydrogen atoms present in cold hydrogen plasma (source of hydrogen) were chemisorbed at the graphene surface. There are reasons to believe that in other experiments,^{107,108} graphene was hydrogenated non-uniformly, which influenced the electronic properties of the final structure.

Indeed, the formation of graphane islands on graphene surface is accompanied by local distortion of its π -system by adsorbed hydrogen atoms; adjacent carbon atoms become more reactive and thus more preferable for hydrogen adsorption.¹⁰⁹ It should be noted that nucleation of graphane can equiprobably occur in both A- and B-sublattices of graphene (see Fig. 1a); this may lead to formation of interfaces between graphane islands. Such interfaces can change the electronic properties of the material (hydrogen chemisorption at the interface is energetically unfavourable).¹¹⁰ Dependences of the electronic properties of hydrogenated graphene on the concentration and arrangement of hydrogen adatoms were studied.^{111,112} In particular, it was established that the electronic properties of partially hydrogenated graphene depend strongly not only on the concentration of adsorbed hydrogen atoms, but also on their arrangement.¹¹²

Hydrogen adsorption strongly affects the electronic properties of graphene even if the hydrogenation degree is relatively low. For instance, adsorption of one H atom per 1 nm² of graphene sheet (a kind of graphene superlattice with 1-nm² unit cell) may open a band gap of 1.25 eV.¹¹³ A 2H-SL superlattice structure was also proposed.¹¹⁴ It represents graphene with ‘lines’ of pairs of hydrogen atoms adsorbed on the surface. These ‘lines’ change the electronic structure of graphene in such a manner that it becomes a semiconductor (Fig. 10a). ‘Lines’ of hydrogen atoms form

graphene nanoroads whose properties depend on the index n that is proportional to the distance between the ‘lines’. Initially, the possibility for such a material to exist was substantiated by the experimentally observed chemisorption of pairs of hydrogen atoms on graphite surface;¹¹⁵ these pairs formed a kind of ‘lines’ on the surface. In such

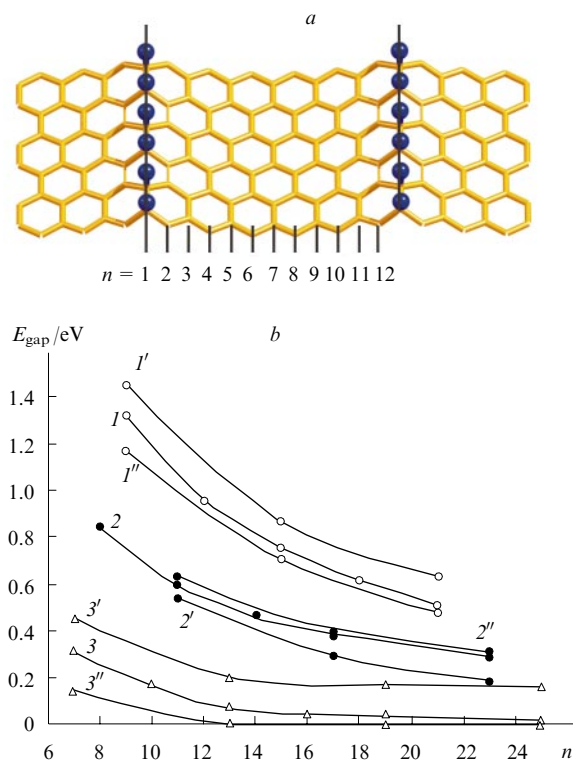


Figure 10. Atomic structure of the (12,0) ‘armchair’ graphene superlattice lined by chains of hydrogen atoms (a) and the band gap of the superlattice plotted vs. index n and vs. mechanical strain (2%) applied along the normal to the hydrogen chains (b).¹¹⁶ Shown are the points corresponding to undistorted chains with the indices $n = 3m$ (1), $3m-1$ (2) and $3m-2$ (3), where m is a positive integer, and the curves for the stretched (1', 2', 3') and compressed (1'', 2'', 3'') structures, respectively.

structures, hydrogen atoms form sp^3 -hybridized bonds and thus distort the graphene lattice. This manifests itself in the surface ‘extension’ (formation of a ‘diamond line’ below the ‘line’ of hydrogen atoms). The electronic properties of graphene nanoroads confined between ‘lines’ of adsorbed hydrogen atoms (see Fig. 10 *a*) are similar to corresponding properties of ‘armchair’ GNRs; *e.g.*, their band gaps oscillate as the separation between the ‘lines’ changes (see Fig. 10 *b*).⁵⁰ The band gap of graphene with ‘lines’ of hydrogen atoms adsorbed on the surface is highly sensitive to mechanical strain, *viz.*, the band gap width changes by 30% at a strain of 2% (Fig. 10 *b*).¹¹⁶

According to spin-state calculations¹¹⁶ of ‘zigzag’ graphene decorated with ‘lines’ of hydrogen atoms (Fig. 11 *a*), antiferromagnetic spin orientation (see Fig. 11 *b*) is energetically more favourable than the ferromagnetic orienta-

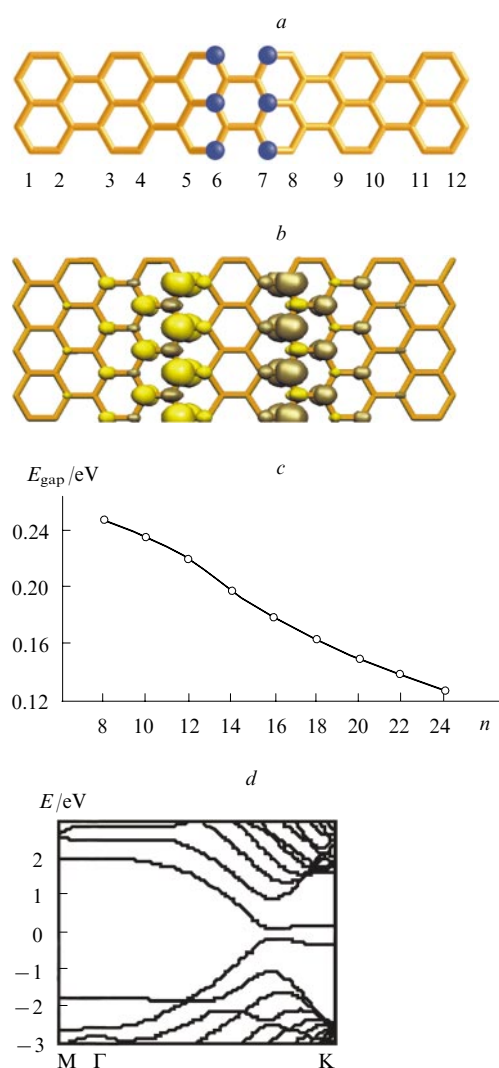


Figure 11. Atomic structure of the (12,0) ‘zigzag’ graphene superlattice lined by chains of hydrogen atoms (*a*), spatial distribution of charges with differently oriented spins (given in different tints of yellow) (*b*), the plot of the band gap of the superlattice *vs.* index n that is proportional to the inter-chain distance (*c*) and example of the energy band structure of the (12,0) superlattice (*d*).¹¹⁶ $E = 0$ is the Fermi level.

tion. This points to a complete analogy between these structures and ‘zigzag’ GNRs for which the antiferromagnetic spin orientation is energetically favourable.⁵³ The band gaps of the ‘zigzag’ superlattices monotonically decreases from 0.25 eV (for structures with a superlattice period of 16.6 Å, $n = 8$) to zero for infinitely long separation between the ‘lines’ of hydrogen atoms, *i.e.*, pristine graphene (see Fig. 11 *c*).

All superlattices have linear spectra along the direction perpendicular to ‘lines’ of hydrogen atoms (ΓM region of the energy band structure), as shown in, *e.g.*, Fig. 11 *d*. This is an indication of high energy barriers that are produced by the sp^3 -hybridized carbon atoms and hamper the motion of electrons along this direction. Therefore, such structures can be treated as parallel electron waveguides (a kind of one-atom thick nanowires).

It is interesting to fabricate superlattices based on graphene with ‘lines’ of hydrogen atoms, where the ‘quasi-metallic’ strip with a narrower band gap is confined between wide band gap strips (Fig. 12 *a*). Note that these can also be pure graphene strips. These structures can be treated as electron waveguides or 2D structures with a heterojunction between two semiconductors with different band gaps (Fig. 12 *b*).⁵⁰

The formation of electron waveguides on graphene can be used to design electronic circuits by controlled hydrogen adsorption on graphene surface.¹¹⁶ A number of structures to play the role of nonlinear elements for such circuits were proposed (Fig. 12 *c*). In these systems, ‘lines’ of hydrogen atoms will form regions with lower conductivity. Theoretical predictions were substantiated experimentally,¹¹⁷ namely, a low-conductivity region was actually observed between the ‘lines’ of hydrogen atoms adsorbed on the upper graphite layer (Fig. 12 *d*).

2H-SL superlattice structures comprising ‘lines’ partially filled with pairs of hydrogen atoms (*e.g.*, in the case of hydrogen adsorption on graphite surface in the course of annealing) can also form on graphene surface.¹¹⁵

To describe superlattices with sparsely arranged pairs of hydrogen atoms, an additional index k equal to the number of carbon rings separating pairs of hydrogen atoms (see Fig. 13 *a–c*) was introduced.¹¹⁸

The band gap width is plotted *vs.* superlattice period along the x axis in Fig. 13 *d*. Calculations of $n \times k$ -2H-SL structures were carried out for $n = 3–12$ and $k = 0, 1, 2, 3$. It was found that E_{gap} decreases as the distance between neighbouring pairs of hydrogen atoms (superlattice period along the y axis) increases. Interestingly, this dependence for the $(3m-1) \times k$ -2H-SL (m is a positive integer) is non-monotonic. These structures behave as semiconductors at $k < 3$ and as semimetals at any nonzero k . The $(3m-1) \times 1$ -2H-SL structures have wider band gaps compared to the $(3m-1) \times 0$ -2H-SL structures.

Graphane regions with sp^3 -hybridized carbon atoms produce rather high energy barriers to the motion of free electrons towards neighbouring graphene fragments. Thus, selective hydrogenation of graphene makes it possible to fabricate materials with controlled electronic properties. This is of particular importance in the light of numerous attempts to apply graphene in nanoelectronics.

The possibility to use hydrogen adsorption to create graphene quantum dots was considered.¹¹⁹ A number of experimental designs were proposed for controlled adsorption on convex regions of a stressed GNR and on various

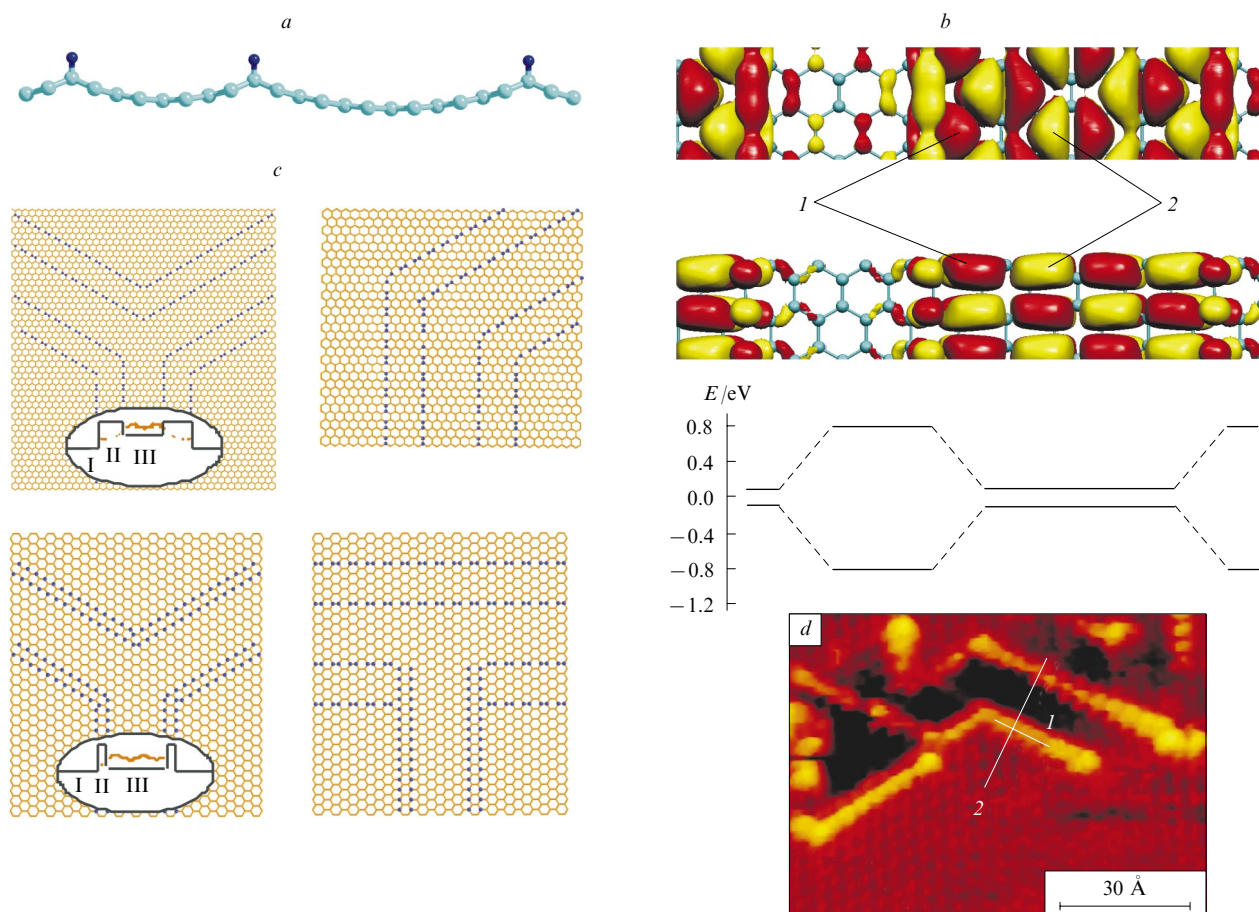


Figure 12. Atomic structure of graphene superlattice with ‘lines’ of adsorbed hydrogen atoms located at different distances from one another (a), the wave function (ψ) distribution at the top of the valence band and at the bottom of the conduction band (1 — $\psi > 0$, 2 — $\psi < 0$) and a schematic illustration of a heterojunction in the superlattice — periodic dependence of the band gap (b);⁵⁰ geometries of hydrogen ‘lines’ adsorbed on graphene surface in the nanoelectronic functional units (c), the insets present the energy barrier schemes [regions: semimetallic graphene (I); wide band gap electron waveguide (II); narrow band gap electron waveguide (III)];¹¹⁶ a SEM image of the surface layer of graphite with ‘lines’ of adsorbed hydrogen atoms (d): region of lower conductivity is given in black, lines 1 and 2 denote directions along and perpendicular to the ‘lines’ of adsorbed hydrogen atoms.¹¹⁷

sites in the structure comprising two overlapped GNRs beyond the intersection region. It was shown that adsorption of hydrogen atoms on convex regions of the GNR is energetically favourable. This leads to the appearance of dielectric graphane nanoislands separating conductive regions. Eventually, a graphane quantum dot with discrete energy levels is formed.

A number of experimental studies on selective hydrogenation of graphene are available. For instance, local desorption of hydrogen from graphane surface under the action of the tip of a scanning tunnelling microscope as the voltage changes from 3.75 to 5 V leads to formation of graphene regions whose surface area increases with the voltage.¹²⁰ This technique makes it possible to create graphene ‘nanoroads’ of different width. Dehydrogenation of graphane is also possible under the action of short (~ 2 fs) laser pulses.¹²¹

The systems thus fabricated can be represented by a GNR confined between high potential barriers originated from graphane.⁵¹ Therefore, one can expect that the electronic properties of ‘nanoroads’ will be similar to those of GNRs. According to calculations, the properties of the

‘armchair’ and ‘zigzag’ nanoroads resemble those of corresponding nanoribbons⁴⁸ and graphene with ‘lines’ of hydrogen atoms adsorbed on the surface.⁵⁰ The band gap energy of ‘armchair’ nanoroads oscillates as the nanoroad width varies and tends to vanish at infinite width (limiting case corresponding to graphene).

Selectively hydrogenated graphene is obtained by hydrogenation of certain regions. A possible method is as follows. Graphene on a crystalline substrate forms a Moiré structure if the lattice parameters of graphene and the substrate are different. Attachment of a hydrogen atom to the carbon atom adjacent to the carbon atoms located above the metal atoms of the substrate involves the metal atoms in chemical interaction and leads to formation of a graphane-like structure.¹²² The drawbacks of this method include the presence of a substrate, difficulties in control of the Moiré structure and the fact that the final material is chemically bonded to the metallic surface, thus being not a true 2D material.

One more approach involves hydrogenation of masked graphene. Various types of mask are available, e.g., hydrogen silsesquioxane,¹²³ a photoresist and PMMA¹²⁴

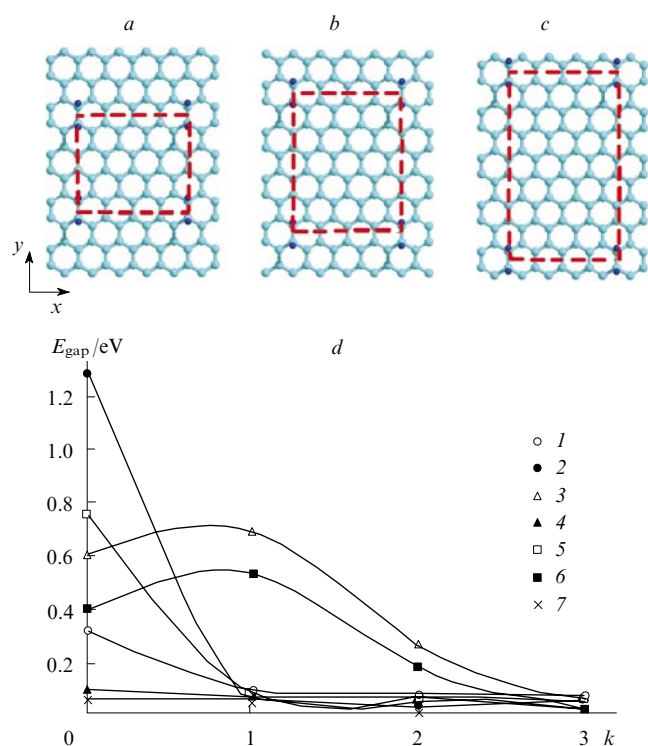


Figure 13. Models for $4 \times k$ -2H-SL with $k = 1$ (a), 2 (b), 3 (c) with 2H pairs loosely adsorbed on graphene (rectangles denote corresponding unit cells) and plots of band gaps vs. k values for $n \times k$ -2H-CP at $n = 6$ (1), 8 (2), 10 (3), 12 (4), 14 (5), 16 (6), 18 (7) (d).¹¹⁸

(Fig. 14). The size of regularly patterned graphene and graphane regions was of the order of $1 \mu\text{m}$. One can hope that further improvement of the technique will enable controlled formation of nanometre-scale graphene–graphane regions.

Stability assessment of the graphene/graphane interface revealed that it is highly stable and gave a value of 1 eV for the energy barrier to diffusion of hydrogen atom from graphane to graphene.¹²⁶ More recently, the barrier height value was corrected upwards to 3,¹⁰⁹ 2.2–2.9¹²⁷ and 2.9–3.2¹²⁸ eV, respectively. Thus, one can expect that a graphane region once synthesized will retain its shape.

Successful hydrogenation of graphene was followed by analysis of the possibility for graphane nanoribbons to exist. Theoretical studies^{129, 130} concerned with hydrogen-terminated ‘zigzag’ and ‘armchair’ nanoribbons. Like graphane, both types of ribbons are wide-band gap semiconductors. The ribbons have wider band gaps than graphane due to the quantum size effect, but this effect weakens as the ribbon width increases and the band gap energy thus decreases and tends to approach the corresponding value for graphane.^{129, 130} Partially hydrogenated GNRs were reported.^{119, 131} In particular, the dependence of the electronic structure of a GNR on the concentration of hydrogen in the case of patterned adsorption was studied.¹¹⁹

Figure 15 shows that an increase in the concentration of hydrogen on the GNR surface is accompanied by the appearance of an electronic spectrum with discrete energy levels. Narrow mini-bands near the Fermi level (see Fig. 15b) indicate that the width of the graphane band is insufficient for quantum dot formation. This leads to a

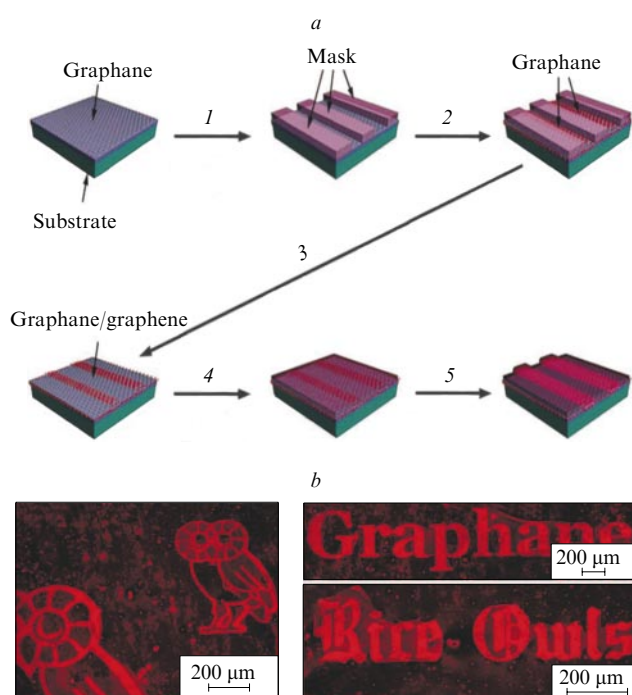


Figure 14. Formation of graphene–graphane structures (a) and experimental results (b).¹²⁴

Patterning (1), hydrogenation (2), removing mask (3), spin-coating dye layer (4) and fluorescence quenching microscopy (5).

The images were obtained using fluorescence quenching microscopy proposed in Ref. 125.

narrow energy barrier through which electron tunnelling from one graphene region to another occurs. Further increase in the concentration of hydrogen adsorbed on graphene causes the separation between the bottom of the conduction band and the top of the valence band in the electronic spectrum to increase (see Fig. 15c–e).

Thus, controlled hydrogenation of graphene nanoregions opens great prospects for the design of graphene-based integrated circuits. However, this requires solving a number of technological problems including controlled fabrication of graphene fragments with nanometre-scale widths as well as atomically precise control of graphene/graphane interfaces that should be smooth and defect-free.

2. Fluorographene

Successful fluorination of graphite was reported a few decades ago. Depending on the experimental conditions and source of fluorine atoms, various stable phases of graphite fluoride were obtained. These are $(\text{CF})_n$, $(\text{C}_2\text{F})_n$ (see Ref. 132) and $(\text{C}_4\text{F})_n$ (see Ref. 133). Probably, some of them represent ultrathin diamond films with fluorinated surface. An analysis of the data on graphite fluoride^{132, 134, 135} and CNTs decorated with fluorine atoms^{136, 137} showed that fluorination of graphene is possible and it was done experimentally.^{95, 138–140} Fluorographene was synthesized in different manner namely, by cleavage of graphite fluoride crystallites placed in a solution in isopropyl alcohol,¹³⁸ in sulfolane¹³⁹ or in DMF¹⁴¹ under sonication; by mechanical cleavage using the ‘Scotch tape’

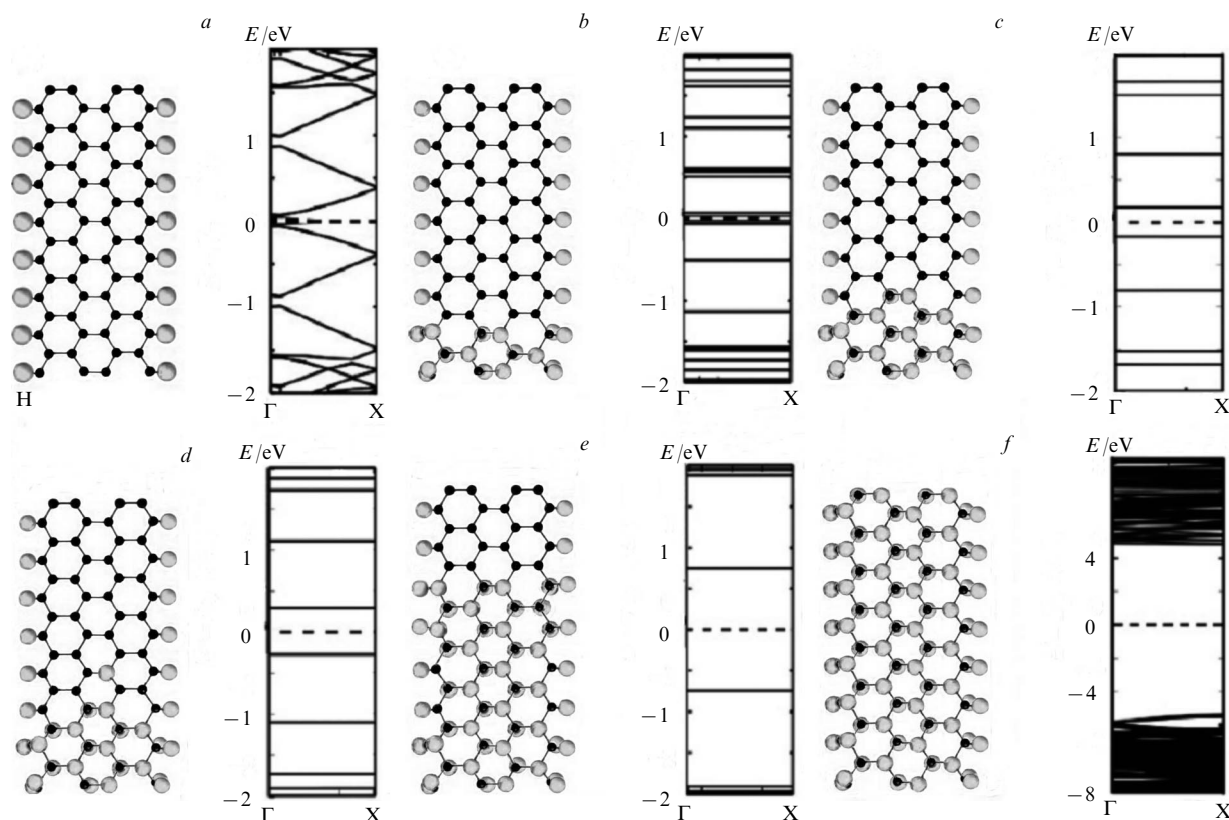


Figure 15. Changes in the electronic properties of a ‘zigzag’ graphene nanoribbon ($n = 4$) at different concentrations of hydrogen atoms.¹¹⁹ The electronic spectrum changes from continuous spectrum of ‘pure’ graphene nanoribbon (*a*) through ‘dispersionless’ spectra of quantum dots with the growing band gap (*b–e*) to the spectrum of dielectric graphene nanoribbon (*f*). Dashed lines denote positions of the Fermi level.

technique;^{95, 142} and by direct fluorination of graphene.^{95, 133, 140, 142}

Phases with different fluorographene/graphene ratios were synthesized. A C_4F phase with fluorine atoms adsorbed on one side of a graphene sheet was obtained.¹⁴² According to calculations, this phase should have a band gap of 2.93 eV.^{52, 142} For the equivalent phase CF , the theoretical band gap values were in the range from 3.0 to 7.5 eV,^{52, 104, 138, 139, 143, 144} (*cf.* experimental values of 2.9,¹³³ 3.0,⁹⁵ and 3.8 eV¹⁴⁰).

Long before the fabrication of fluorographene,^{145, 146} it was predicted that ‘armchair’ fluorographene (see Fig. 9) will be the most stable polymorph of graphene similarly to hydrogenated graphene.

It was shown⁵² that the electronic properties of graphene nanoroads with ‘armchair’ and ‘zigzag’ edges are fundamentally different. However, unlike graphane,⁵¹ the narrowest nanoroads in fluorographene are energetically unfavourable because of lattice distortion produced by the fluorine atoms. Theoretical prediction of an inverse dependence of the fluorographene band gap energy on the width of graphene nanoroads was confirmed experimentally.¹⁴⁷

Fluorination of graphene occurs rapidly owing to almost barrierless chemisorption of fluorine on graphene. Unfortunately, the process is accompanied by the degradation of graphene because large fluorine atoms produce significant structural distortions in the material. Therefore, fluorographene is difficult to use in nanoelectronics. How-

ever, taking into account high chemical and thermal stability of the substance, one can assume that it will find applications as dielectric nanomaterial, *e.g.*, insulator in electric circuits.

3. Graphene oxide

Graphene oxide is yet another promising material that has attracted considerable recent attention of researchers. Information on graphene oxide is summarized in some publications, Refs 13 and 148–150 being of particular interest. In this Section, we will briefly outline methods for the synthesis of graphene oxide in order to provide the state of the art to the reader.

Graphene oxide can be obtained by the oxidation of graphite by strong oxidants (H_2SO_4 , HNO_3 , $KMnO_4$, $KClO_3$, $NaClO_2$) followed by exfoliation. Currently, there are three main methods for the synthesis of graphite oxide. Two of them were proposed more than 100 years ago by Brodie¹⁵¹ and Staudenmaier.¹⁵² There is also a more recent Hummers method.¹⁵³ These methods involve graphite reactions with concentrated sulfuric acid, fuming nitric acid and potassium perchlorate (Staudenmaier), with fuming nitric acid and potassium chlorate (Brodie) and with anhydrous mixture of sulfuric acid, sodium nitrate and potassium permanganate (Hummers).

Graphene oxide is a nonstoichiometric compound with a C:O ratio that varies from 2.0 to 2.9; this hampers structural description. A number of structural models were

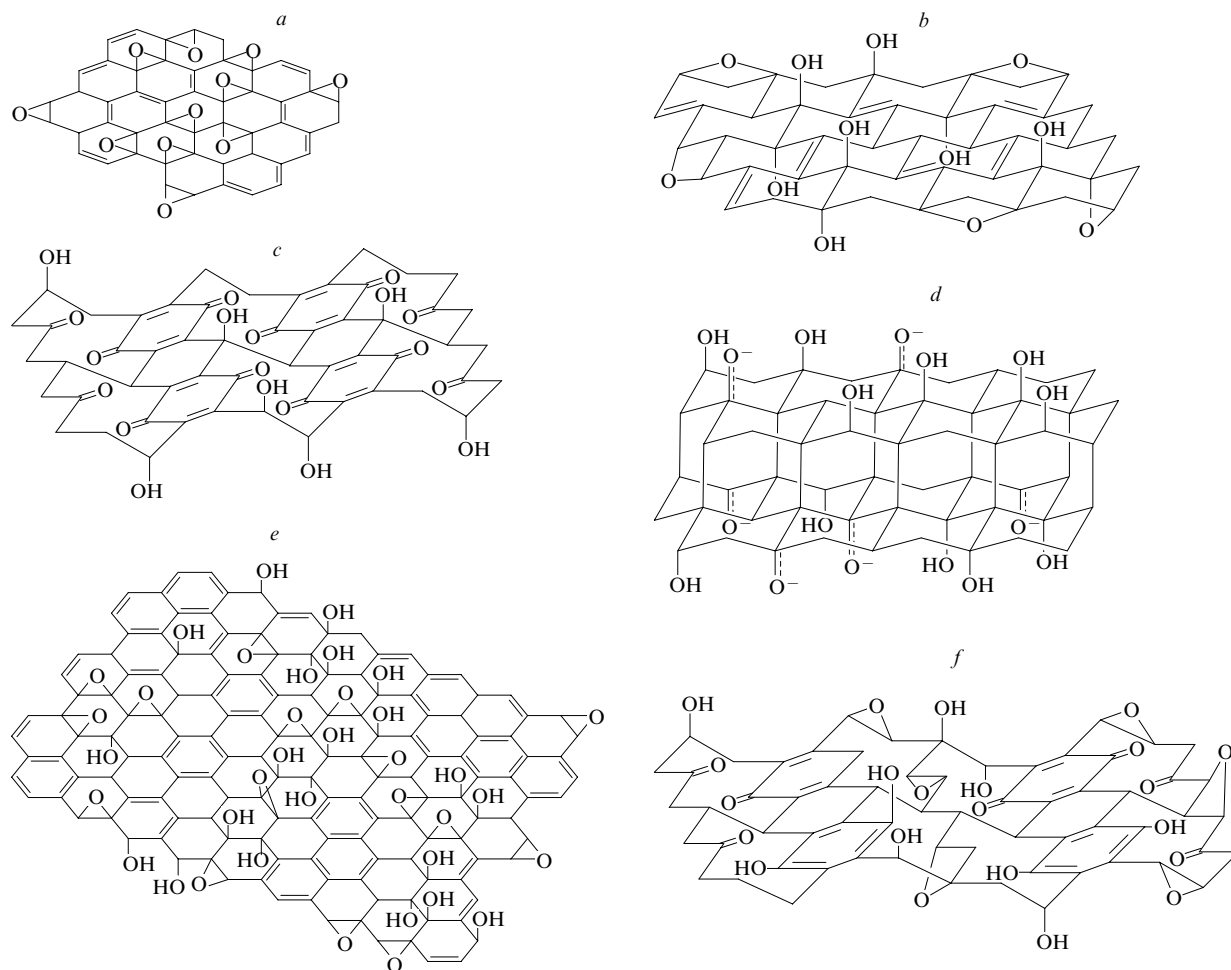


Figure 16. Various structures of graphene oxide.

The structures were taken from Refs 155 (a), 155 (b), 156 (c), 157 (d), 158 (e) and 159 (f).

proposed (Fig. 16). It is believed¹⁵⁴ that graphene oxide is comprised of epoxy groups distributed across the graphene surface and can be described by the molecular formula C_2O . Based on information on the presence of hydrogen atoms in graphite oxide, it was assumed¹⁵⁵ that not only epoxy, but also hydroxyl groups should be attached to graphene surface and most carbon–carbon bonds should be sp^3 -hybridized. In this model, patterned functionalization was considered. The model proposed in another study¹⁵⁶ includes patterned attachment of quinoid groups to graphene. Based on the experimental data on fluorination of graphite, an ultrathin diamond structure (see next Section) decorated with hydroxyl groups was proposed.¹⁵⁷ In the most widely used model,¹⁵⁸ the surface of graphene bears randomly distributed epoxy (1,2-ether) and hydroxyl groups while the edges are terminated by carboxyl, carbonyl and lactyl groups. One more model¹⁵⁹ treats a corrugated quinoid structure formed by *trans*-connected cyclohexyl units functionalized with tertiary alcohol and 1,3-ether residues.

It is difficult to give an unambiguous description of the electronic structure of graphene oxide because of random distribution of epoxy and hydroxyl groups on the graphene surface. It was proposed to consider graphene oxide as combination of regions formed by sp^3 - and sp^2 -hybridized

carbon atoms.¹⁶⁰ Almost fully oxidized graphene is a light-brown material having the properties of a dielectric and a band gap of 2.4 eV.¹⁶¹ The oxidation state of graphene influences the width of the band gap.^{161,162} It was found¹⁶¹ that, depending on the oxidation state, the band gap energy E_{gap} of graphene oxide can vary from 1.7 to 2.4 eV. The intensity of the experimentally observed^{162,163} blue photoluminescence of graphene oxide appeared to be dependent on the degree of chemical reduction. These data were confirmed by the results of theoretical simulation of the dependence of the band gap width on the oxidation state of graphene.^{164–166} A constitutional diagram was constructed¹⁶⁶ for the ternary system $C_{1-x-y}-(C_2O)_x-[C_2(OH)_2]_y$ ($1-x-y$ is the proportion of sp^2 -hybridized carbon atoms, x is the proportion of epoxy groups and y is the proportion of 1,2-hydroxyl pairs) and it was shown that epoxy groups tend to form ribbons confined between sp^2 -hybridized regions.

Not only the oxidation of graphene, but also the reverse process, *i.e.*, reduction of graphene oxide is of considerable importance. The latter process opens prospects for large-scale production of graphene. The material is usually called reduced graphene oxide; as a rule, it contains numerous defects.

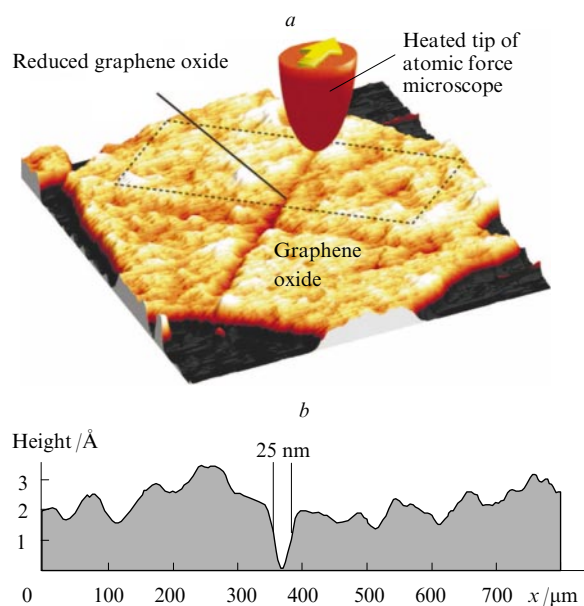


Figure 17. Topography image of reduced graphene nanoroads in graphene oxide (a) and profile of graphene oxide with a graphene nanoroad 25 nm wide (b).²⁰⁹

Reduction methods can be divided into chemical and thermal ones.¹⁵⁰ Chemical reduction is attained using a wide variety of reducing agents, such as diamide,^{167–173} alcohols,^{174, 175} sodium borohydride,^{176–179} hydroiodic acid¹⁸⁰ and its mixtures with acetic acid,^{180, 181} sodium hydroxide¹⁸² and potassium hydroxide,¹⁸³ powdered iron¹⁸⁴ and aluminium,¹⁸⁵ ammonia,^{186, 187} hexylamine,¹⁸⁸ sulfur-containing compounds (NaHSO₃, Na₂SO₃, Na₂S₂O₃, Na₂·9H₂O, SOCl₂, SO₂,¹⁸⁹ Na₂S₂O₄¹⁹⁰), hydroxylamine hydrochloride,¹⁹¹ urea,¹⁹² lysozyme,¹⁹³ vitamin C,¹⁹⁴ *N*-methyl-2-pyrrolidone,¹⁹⁵ polymerized norepinephrine,¹⁹⁶ bovine serum albumin,¹⁹⁷ TiO₂ nanoparticles^{198, 199} and manganese dioxide.²⁰⁰ Biodegradation of graphene oxide is also used.²⁰¹ Thermal reduction methods are based on heating of graphene oxide under the action of microwave radiation,^{202–204} flashing light,²⁰⁵ laser,²⁰⁶ plasma,²⁰⁷ electric current,²⁰⁸ heated tip of atomic force microscope²⁰⁹ in various atmospheres (ultrahigh vacuum, Ar, H₂, NH₃).^{210, 211}

Noteworthy is a method²⁰⁹ that makes it possible by tip of atomic force microscope to form graphene nanoroads in graphene oxide and fabricate structures similar to the predicted structures of graphane and fluorographene (see Fig. 17). This offers prospects for application of graphene oxide with low content of defects in the design of integrated circuits.

4. Doping of graphene

The properties of graphene can be manipulated using not only hydrogen adsorption on its surface, but also doping with boron and nitrogen. In the experiment,²¹² graphene on a copper substrate was doped with nitrogen by chemical vapour phase deposition using an ammonia/methane mixture; a doping degree of 8.9 % was attained. Yet another approach to doping graphene with nitrogen is to use arc discharge:²¹³ a graphene specimen was placed between

graphite electrodes in ammonia atmosphere. The concentration of nitrogen was at most 1 mass %. A similar technique was used in another study²¹⁴ with the exception that the graphene specimen was placed in an arc discharge in the presence of hydrogen and pyridine (or hydrogen and ammonia); the doping degree was 1%.

Also, graphene was doped with boron using arc discharge in hydrogen/diborane atmosphere or using boron-enriched graphite as electrodes. The doping degree was 1.2% and 3.1% in the former and in the latter case, respectively.²¹⁴ Highly oriented pyrolytic graphite was doped²¹⁵ with boron using B₄C powder: at high temperature (>700 °C), diffusion of boron atoms began. A study by scanning tunnelling microscopy and Raman scattering revealed that replacement of carbon atoms by boron in graphite was accompanied by the formation of defects and structural disordering.²¹⁶

Not only doping with certain elements, but also fabrication of hybrid graphene/hexagonal boron nitride structures has been subject of wide speculation. This is first of all due to the close lattice parameters and to the possibility of formation of polar covalent bonds between carbon, boron and nitrogen atoms. Various types of hybrid structures comprised of carbon, boron and nitrogen were analyzed by the Monte Carlo method.²¹⁷ It was found that B and N atoms tend to segregation with the formation of h-BN islands. This result was confirmed experimentally by Ajayan and co-workers,²¹⁸ who pioneered in the synthesis of graphene/h-BN material on a copper substrate by chemical vapour phase deposition (Fig. 18 a,b) using methane as source of carbon and NH₃–BH₃ as source of boron and nitrogen. In another study,²¹⁹ graphene/h-BN hybrid films were grown on the Rh(111) surface by the two-step method from the same precursors. First, h-BN islands were grown on the Rh(111) surface and then graphene was synthesized and filled regions between the h-BN islands. The authors evaluated the ratio of interfaces with the ‘zigzag’ and ‘armchair’ edges (77.64/22.36) and concluded that the ‘zigzag’ edge is more preferable in the graphene–h-BN system.

A number of studies^{220, 221} are devoted to models for quantum dots (alternation of fragments of CNTs and boron nitride nanotubes) and theoretical research on the electronic properties of graphene–h-BN systems. A study²²² on graphene quantum dots in an h-BN layer revealed that graphene quantum dots with ‘armchair’ edges are the most energetically favourable. Also, it was established that the electronic properties depend on the size of the quantum dot. Graphene nanoroads in h-BN were investigated by Bhowmick *et al.*²²² and Ding *et al.*²²³ It was shown that their properties are similar to those of GNRs,^{46–48} CNTs,⁴⁹ graphene patterned with regularly adsorbed ‘lines’ of hydrogen atoms,⁵⁰ graphene nanoroads in graphane⁵¹ and fluorographene⁵² due to manifestation of a common effect, *viz.*, the appearance of a finite number of states in the Brillouin zone owing to conversion of 2D graphene to a quasi-1D nanoroad (h-BN regions that confine the nanoroad can be treated as infinitely high barrier because of a wide band gap of about 5.5 eV²²⁴).

The graphene–h-BN systems in question are candidates for being utilized not only as elements of 2D electronics, but also in highly sensitive biochemical sensors.²²³ However, similarly to some other cases, these structures are difficult to synthesize because of the need for atomically precise control of graphene/boron nitride interfaces. Presently, two

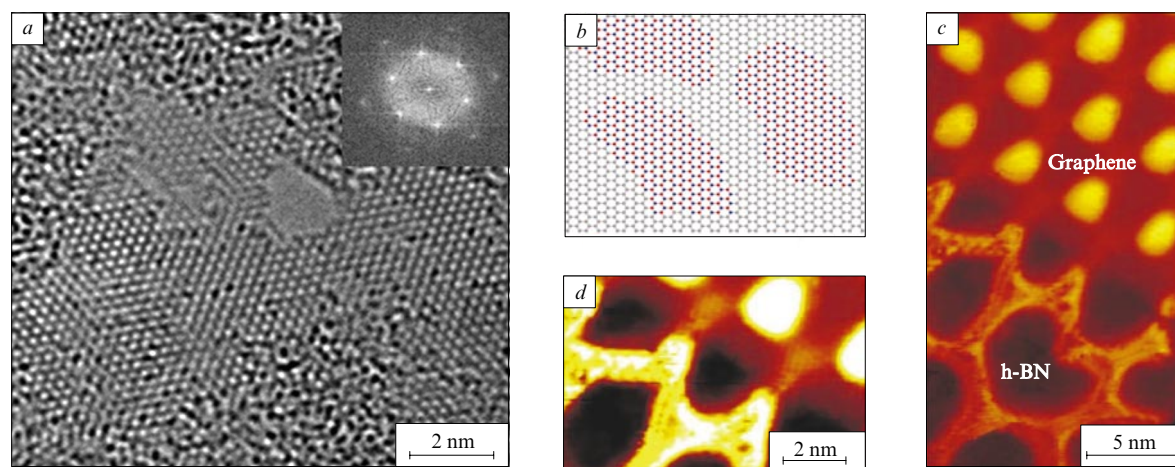


Figure 18. High-resolution STM images of graphene–h-BN system (*a*) (inset: the fast Fourier-transform of the image, which confirms a hexagonal structure of individual layer); atomic model for the graphene–h-BN system (*b*),²¹⁸ and images of graphene/h-BN interfaces (*c, d*).²²⁵

studies on the topic are available. Sutter *et al.*²²⁵ formed a controlled interface using inhomogeneities of the Ru(0001) surface on which the graphene–h-BN layer was formed (Fig. 18 *c, d*). Levendorf *et al.*²²⁶ fabricated the hybrid interface by growth of h-BN film around a preliminarily cut graphene region.

In addition to selective functionalization of graphene surface (see above) extended regions with nonzero band gaps can be formed mechanically. It was shown theoretically²²⁷ and observed experimentally²²⁸ that strong periodic bending of graphene sheets causes the appearance of semiconductor nanoroads with a band gap of >0.5 eV in the graphene structure. This technique is promising because it enables the fabrication of semiconductor circuits.

Summing up, various methods for graphene functionalization have been developed to date. Graphene hydrides, fluorides and oxides having the properties of semiconductors were synthesized. Of particular interest are hybrid nanostructures in which some graphene nanoregions are functionalized or doped and exhibit the properties of semiconductors. In spite of a large number of theoretical studies with predictions of the properties of such structures, relevant experimental data are scarce. This is first of all due to the difficulties in atomically precise control of interfaces between graphene and the modified nanodomains whose size and shape govern particular properties of the hybrid materials.

5. Ultrathin diamond-like films

Graphane, as well as fluorographene, can be treated not only as graphene derivative obtained by functionalization of its surface, but also as the first representative of a series of diamond-like films whose surface is decorated with hydrogen or fluorine atoms, respectively. Hypothetical structures of C_nH films ($n = 2, 3 \dots$) formed upon hydrogenation of the surfaces of a stack of graphene sheets with the formation of ‘diamond-like’ bonds between the constituent atoms were named ‘diamanes’.²²⁹ Therefore, graphane and ultrathin films can be considered as representatives of a continuous series of diamond-like quasi-2D structures with gradually increasing thickness.

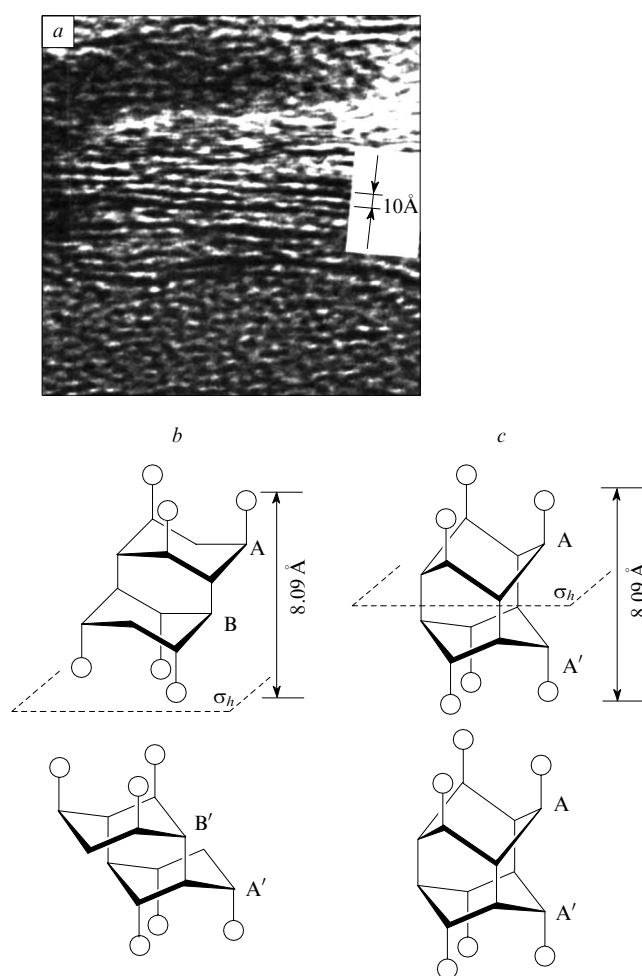


Figure 19. Electron micrograph of $(C_2F)_n$ (*a*) and structural models for stacking patterns of carbon difluoride in adjacent layers AB/B'A' (*b*) and AA'/AA' (*c*).¹³⁴ σ_h is a mirror plane perpendicular to the principal symmetry axis.

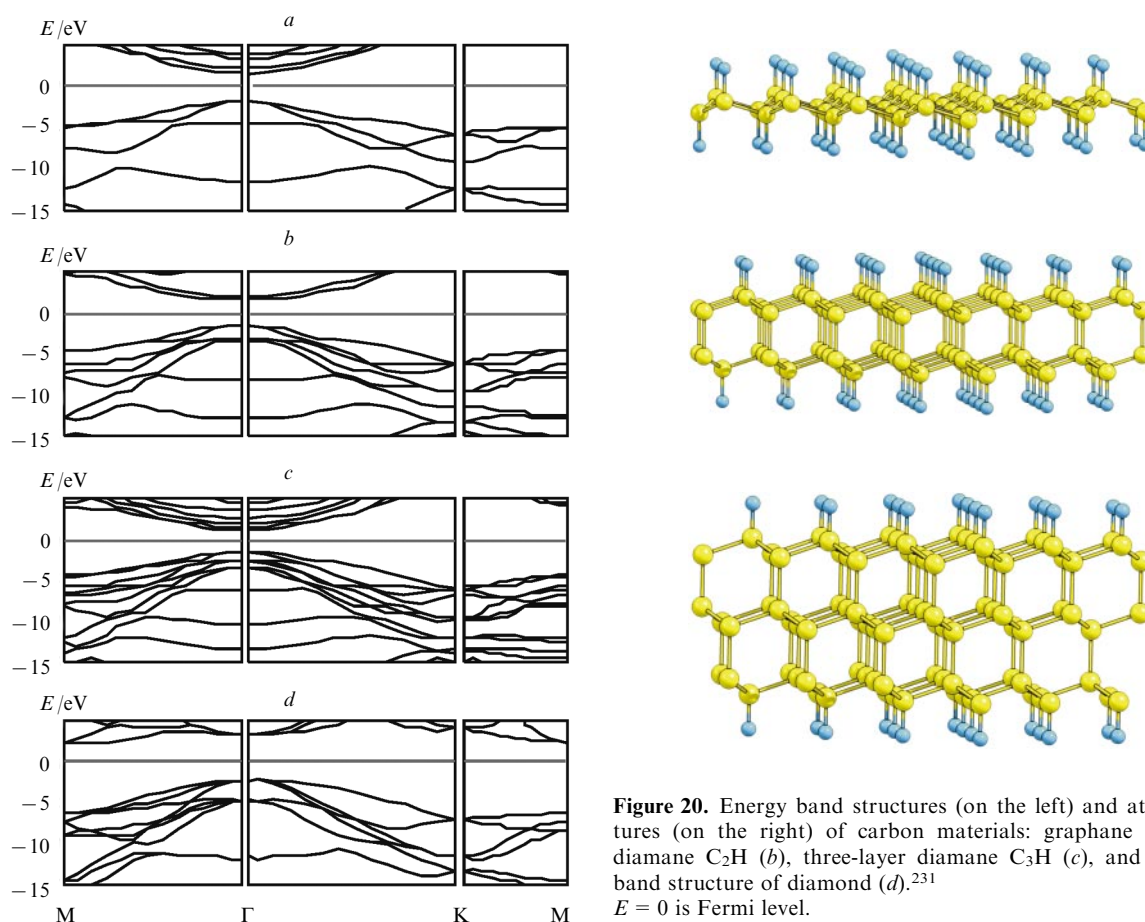


Figure 20. Energy band structures (on the left) and atomic structures (on the right) of carbon materials: graphane (a), bilayer diamane C_2H (b), three-layer diamane C_3H (c), and the energy band structure of diamond (d).²³¹ $E = 0$ is Fermi level.

An experimental study on the preparation of a layered material with C_2F stoichiometry by fluorination of graphite was reported as long ago as 1979.¹³² More recently, the structure of the material was interpreted as a stack of C_2F layers,¹³⁵ which was substantiated by the presence of only sp^3 -hybridized bonds between carbon atoms and between carbon and fluorine atoms.¹³⁴ Two stacking sequences, AA' and AB (Fig. 19) corresponding to the lonsdaleite and diamond structures with C_6 and C_{3h} symmetry, respectively, are possible for the material.

According to Mitkin,²³⁰ the C_2F model with close hexagonal (not orthorhombic¹³²) stacking sequence AB/B'A'/AB and $P6m2$ space group ($a = b = 2.50$, $c = 16.2 \text{ \AA}$)¹³⁴ corresponds to an interplanar spacing of 8.09 \AA and a pycnometric density of 3.28 g cm^{-3} , which is 20%–25% higher than the density of the fluorine-rich compound $(CF_{1.0})_n$.¹³² Light-grey colour, low specific resistance ($\sim 10^{14} - 10^{15} \text{ \Omega cm}$), as well as the chemical shift and the second moment of the ^{19}F NMR spectrum of a C_2F specimen^{132,134} indicated that the natures of the C–F bonds in this compound and in $CF_{1.0}$ are similar. From this it followed that C–F bonds in C_2F and in fluorination products of petroleum coke¹³² that is compositionally close to C_2F are covalent.

The material C_2F (and hypothetical C_2H) represents a stack of layers that are held together through van der Waals forces (Fig. 19). Probably, C_2F layers can be cleaved micro-mechanically similarly to graphene; this will make it possible to prepare diamond-like films a few nanometres thick. Theoretical studies^{146, 231, 232} predict that these structures

should exhibit unique mechanical, optical and electronic properties that are governed by the surface and quantum effects.

For instance, ultrathin diamond-like films bearing hydrogen and fluorine adatoms have similar, diamond-like energy band structures (Fig. 20).^{146, 231} Also, unlike crystalline diamond, these films have a direct band gap and thus can be used as laser active media.²³¹

The mechanical properties of diamanes are also similar to those of diamond (Table 1, see also Ref. 233). However, owing to their nanostructural nature, C_2H films demonstrate high elasticity, namely, the limit deflections of C_2H and graphane membranes with a radius of 30 \AA are close, being equal to 7.6 and 8.9 \AA , respectively.²²⁹

It is assumed that diamane can be formed from bilayer graphene placed in hydrogen plasma discharge. Under appropriate conditions (pressure and temperature), chemisorption of hydrogen atoms occurs on both sides of

Table 1. Velocities of transverse (v_{TA}) and longitudinal (v_{LA}) acoustic waves in graphane and diamanes with diamond stacking sequences.²³¹

System	Velocity/ 10^3 m s^{-1}	
	v_{TA}	v_{LA}
Graphane	12.0	17.7
C_2H	12.1	17.8
C_3H	12.2	18.0
Diamond crystal (experiment)	12.4	18.3

graphene surface.²²⁹ A carbon atom of the ‘upper’ graphene, which is located off a corresponding C atom of the ‘lower’ graphene and, therefore, has freedom to move, goes out of plane owing to sp^3 -hybridization after attachment of a hydrogen atom. Three neighbouring carbon atoms are displaced downward. Atomic rearrangement in the ‘lower’ graphene occurs analogously. As a consequence, sp^3 -hybridization of carbon atoms from adjacent stacked layers occurs. This leads to the formation of the diamane nucleus.^{229, 234}

Identification of the final structures is an important step in the experimental studies on the synthesis of ultrathin diamond films. Indeed, multilayer graphene, the starting material for ultrathin diamond films, is assumed to have different types of stacking sequences^{229, 231, 235} (AA' and AB).¹⁰⁸ It follows that the number of possible diamane polytypes will increase with increasing the number of layers (and the number of possible combinations of stacking sequences) in the starting material. Therefore, experimental methods are required to determine the number of layers and the structure of diamane. Here, Raman scattering may appear to be useful.²³⁶ This method was used to determine the number of layers in the structures of single-layer and multilayer graphene from the shape, intensities and positions of peaks in the Raman spectra.²³⁷ Also, the stacking type of three-layer graphene was determined unambiguously.²³⁸

A stack of graphene sheets can be converted to a material where carbon atoms may have both three and four nearest neighbours or, probably, only four nearest neighbours as in diamond.²³⁹ The tensile strength of such a material may exceed a value of 5.6 GPa, the world record in strength known for carbon nanofibres.

Diamane C_2H (or C_3H) is formed from two (or three) graphene layers by hydrogenation of graphene. This nanometre-thick diamond-like film should be significantly different from graphene and graphane in electrical and mechanical properties and manifest the properties of a semiconductor or even superconductor on doping with certain atoms. Diamane films can find application as ultrathin, high-strength dielectric layers.

IV. Graphene-based composites

Recently, experimental and theoretical studies on graphene-based composites have been reported. Like CNTs,²⁴⁰ such composites are attractive to improve the mechanical (rigidity, tensile strength and hardness) and conducting properties of materials for supercapacitors and polymer composites,²⁴¹ woven fabrics and flexible touch screens. For instance, graphene-containing composites based on polymers²⁴¹ and silica,²⁴² as well as graphite oxide/multi-walled CNT films²⁴³ were synthesized.

Probably for the first time, graphitic nanoflakes were grown on the surface of multi-walled CNTs used as substrate by plasma-assisted chemical vapour phase deposition in 2005.²⁴⁴ The procedure involved the synthesis of arrays of micrometre-scale multi-walled CNTs, coating them with iron nanoparticles and subsequent growth of graphitic nanoflakes. Since the surface area of the material increased from 100 to 130 $m^2 g^{-1}$, it was proposed as a candidate for utilization in supercapacitors. However, neither electronic properties of this composite nor types of graphene attachment to CNTs were reported.

A pillared graphene–multi-walled CNTs composite was for the first time synthesized in 2008.²⁴⁵ Since then, a number of studies on the design of related materials were reported and the structures comprising covalently^{246, 247} or molecularly^{247, 248} bonded single-walled CNTs and graphene were simulated.

Below we will consider methods for the synthesis and the results of research on the properties of pure carbon graphene–CNT composites to illustrate their improved mechanical and electronic properties compared to those of individual CNTs or graphene. These composite materials have a great potential for future applications.²⁴⁷

1. Methods of synthesis of graphene–CNT composites

Many studies considered below were often carried out using graphite oxide as the starting material that was reduced to graphene.

A hybrid film comprising graphite oxide and multi-walled CNTs was reported in 2008.²⁴³ Graphite oxide powder was sonicated for 1 h at room temperature. Multi-walled CNTs decorated with hydroxyl groups were dissolved in DMF under sonication for 1 h at room temperature and mixed with graphene oxide. Then, the mixture was placed on a glassy surface and dried over a period of 24 h at 100 °C. The thickness of the film thus fabricated was controlled by monitoring the volume of the mixture placed on the glassy substrate (actually, the film thickness varied from 2 to 8 μm). The electrical resistance of the film decreased as the content of multi-walled CNTs in the composite and the film thickness increased.

Yet another route to composite structures proposed in 2009 involves self-assembly of graphite oxide/multi-walled CNTs bilayer films.²⁴⁸ To this end, graphite oxide obtained by the Hummers method was exfoliated in distilled water under sonication. To prepare a film, a SiO_2/Si substrate was immersed in the solution of graphite oxide for 1 h, washed with water and ethanol and dried in nitrogen stream. The treated substrate was placed in aqueous solution of amidated multi-walled CNTs. To reduce graphene oxide to graphene, the film was immersed in hydrazine for 24 h, washed with water and ethanol, dried in nitrogen stream and heat treated at 125 °C for 15 min. A scheme of the synthetic procedure is shown in Fig. 21. Then, the film was reduced in solutions of hydrazine monohydrate with different concentrations of DMF at 80 °C for 24 h and annealed at 500 °C in argon atmosphere to form graphene sheets and thus abruptly increase the conductivity of the film by a few orders of magnitude. An analysis of the AFM and SEM images revealed a homogeneous structure of the film. The highly conductive material thus obtained exhibited high mechanical strength indicating a long operating life.

A pure carbon structure consisting of graphite layers attached to open ends of CNTs was for the first time synthesized by chemical vapour phase deposition²⁴⁵ using a silicon substrate coated with a catalyst (cobalt and titanium nitride) film. In the heating step, the substrate was placed in a low-pressure chamber (10^{-2} Pa). An argon/acetylene mixture at a pressure of 1000 Pa was used as the source of carbon. The temperature of the substrate was 510 °C, the composite growth duration was 10 min and the growth rate was about 670 $nm min^{-1}$. A SEM image of the composite is shown in Fig. 22a and the model of its structure is presented in Fig. 22b. The width of the graphene sheets varied from 17 to 38 nm, being dependent on

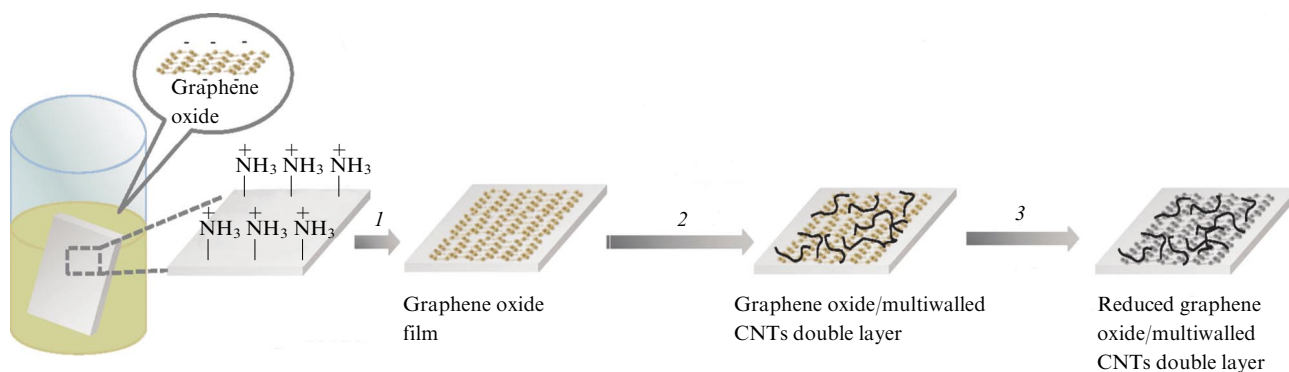


Figure 21. Fabrication of bilayer films.²⁴⁸

Aminated SiO_2/Si substrate is placed in aqueous solution containing graphene oxide (1); deposition of aminated multi-walled CNTs on the substrate coated with graphene oxide film (2); reduction and subsequent annealing (3) result in a reduced graphene oxide/multiwalled CNTs double layer.

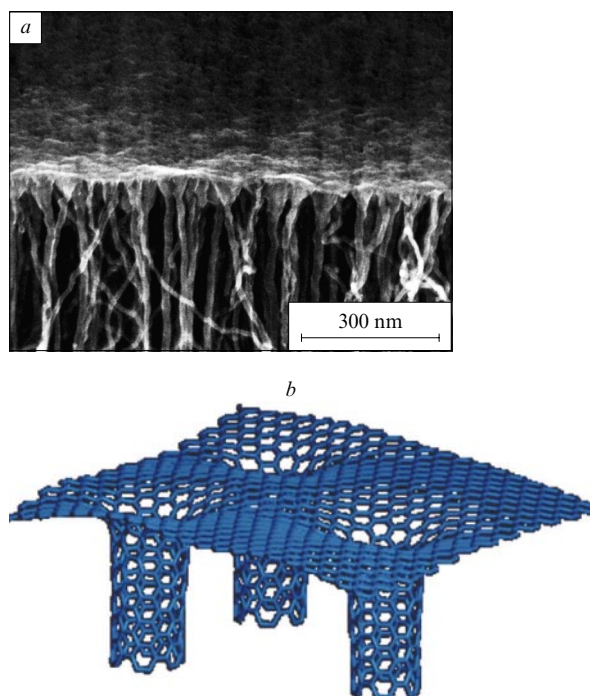


Figure 22. A SEM image of a composite comprising graphene sheets (top) and CNTs (bottom) (a) and model for attachment of CNT to graphene (b).²⁴⁵

The structure is entirely built of sp^2 -hybridized carbon atoms.

the width of the supported catalyst layer. All CNTs thus grown appeared to be multi-walled with an average diameter of 11.9 nm. The new composite was named ‘pillared graphene’. It exhibits good electrical and thermal properties in all directions and is expected to have various applications in electronics.

A nanostructure similar to ‘pillared graphene’ was grown on graphite oxide using the same method under different conditions (600 °C, pressure 5 Torr, in a $\text{C}_2\text{H}_2 + \text{H}_2 + \text{NH}_3$ gas flow).²⁴⁹ The growth of CNTs was accompanied by reduction of graphite oxide to graphene. The conductivity of the structure reached a value of

1800 S m^{-1} . The films appeared to be readily stretchable and flexible and could be transferred to other substrates. Bending of the material led to an increase in its electrical resistance probably due to changes in the mutual position of graphene layers. After a few bending cycles, the electrical resistance of the material increased but then recovered the original value. After 1000 bending cycles, the resistance of the film increased by only 1%.

A structurally similar composite was reported by Hauge and co-workers.²⁵⁰ The role of substrate was played by thermally expanded graphite (grafoil) or carbon fibres coated with 1-nm-thick iron layer used as catalyst. Then, an Al_2O_3 overlayer 5 nm thick was deposited on the substrate. This led to formation of iron nanoislands. The composite was formed at a pressure of 1.4 Torr and a temperature of 750 °C in $\text{H}_2 + \text{H}_2\text{O} + \text{C}_2\text{H}_2$ stream ($400 + 2 + 2 \text{ cm}^3 \text{ min}^{-1}$, respectively). These conditions were optimum for rapid growth of two- and multi-walled CNT forest. A scheme of the synthesis of the composite is shown in Fig. 23 a. The growth mechanism was named ‘Odako’ (a giant kite in Japanese), because the Al_2O_3 layer detached from the substrate during the growth. The CNT diameter distribution in the composite was plotted using the results of a transmission electron microscopy (TEM) study of the composite.

A similar approach was used in another study;²⁵¹ however, unlike the preceding case, iron clusters were deposited on graphene. Examination by electron microscopy revealed narrow (3 to 7 nm in diameter) and long (from 3 to 250 μm) single-, double- and three-walled CNTs attached to graphene. The ohmic character of the CNT/graphene contact is of particular importance for various applications of these composites in electronics, because conventional CNT–metal composites have a barrier to charge transfer.

One more carbon composite was synthesized in two steps by chemical vapour phase deposition.²⁵² First, single-walled CNTs were grown on iron-covered silicon substrate (900 °C, 10 min). Next, graphene flakes were grown on CNTs. It was established that no covalent bonds with graphene are formed owing to chemical inertness of untreated CNTs.

A method for preparation of hybrid films by CNT growth between graphene layers was reported.²⁵³ Graphite oxide layers with uniformly distributed organocobalt agents

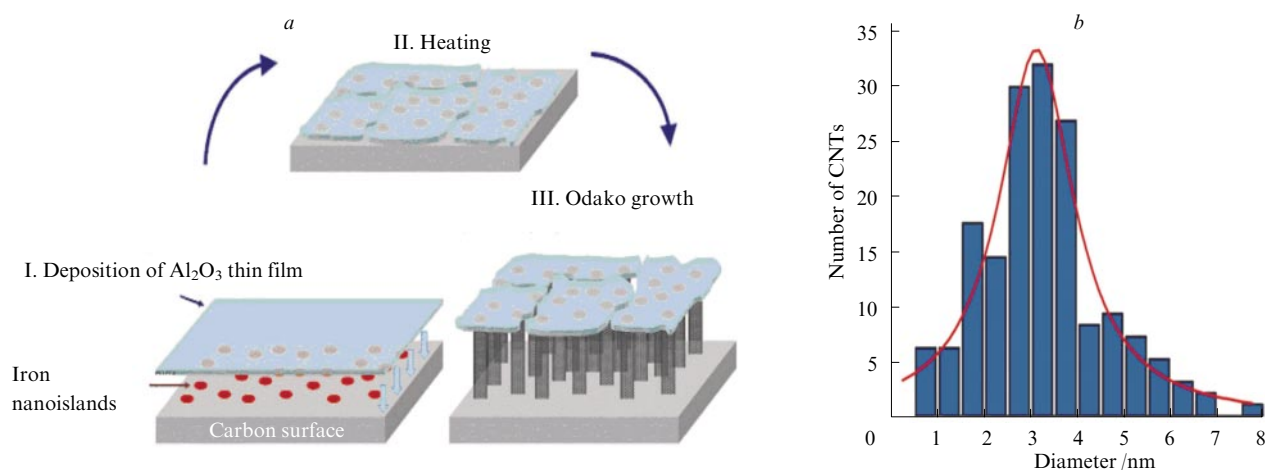


Figure 23. Scheme of the synthesis of a composite (a) and the CNT diameter distribution in the composite containing 164 nanotubes (b).²⁵⁰

[e.g., C₂Co₂(CO)₆] were placed in a C₂H₂ + H₂ + Ar flow at 900 °C for 5 min. Graphite oxide was reduced, while cobalt residues were removed by hydrochloric acid. Carbon nanotubes grown between graphene layers connected them; this improved the mechanical properties of the composite.

A graphene/multi-walled CNT hybrid film was prepared.²⁵⁴ Graphite oxide was chemically reduced in hydrazine in the presence of a stabilizer. A photograph of the solution is shown in Fig. 24a and the AFM images of irregularly shaped graphene layers up to a few micrometres long and up to 2.5 nm thick are presented in Fig. 24b. The composite film self-assembled upon immersion of positively charged graphene in the solution of negatively charged multi-walled CNTs. The film was prepared as follows: carbon black containing multi-walled CNTs was heated to 600 °C for 2 h and then centrifuged in hydrochloric acid for 24 h. The residue was triply washed with deionized water, dried and sonicated in a mixture of nitric and sulfuric acids for 24 h. The powder thus obtained was washed with deionized water, triply centrifuged and dried again in nitrogen stream. Then, nanotubes were dissolved in deionized water. Further steps of the experiment are shown in Fig. 24c.

Positively charged graphene was prepared by adsorption of water-soluble polyethyleneimine chains (step 1). Then,

graphene supported on a substrate was repeatedly immersed in the acid-oxidized solution of negatively charged multi-walled CNTs (step 2) and successive self-assembly of a homogeneous film consisting of interconnected carbon structures occurred. Different types of substrates including silicon, iridium oxide, tin, *etc.* were tested. After that, the composite was heat treated at 150 °C for 12 h (step 3). The thickness of the dried film varied from 0.5 to 5 μm. The iridium oxide and tin substrates covered with the carbon film were used as electrodes and the *I–V* curves were measured for both of them at room temperature. These structures may find application in high-performance supercapacitors. Mention was made that the technique enables fabrication of films with large surface area.

A composite comprising pristine and almost perfect single-walled CNT and graphene was studied.²⁵⁵ It was prepared by separately grinding CNTs and graphite powder in *N*-methyl-2-pyrrolidone under sonication for 10 min and 18 h, respectively. Then, the solutions of the components were mixed in different ratios and sonicated for 18 h. The mixtures thus obtained were filtered and dried initially at room temperature, then at 60 °C for 24 h and finally *in vacuo* at 100 °C also for 24 h. The thickness of the films thus prepared varied from 100 to 500 μm. The dependence of the Young modulus (*Y*) on the content of graphene in the

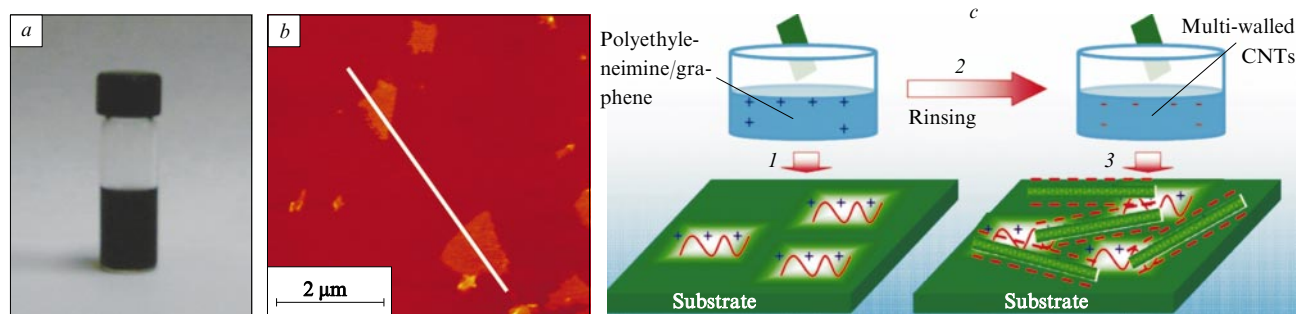


Figure 24. Photograph of aqueous solution of reduced graphite oxide (a), its AFM image (b) (individual graphene flakes are clearly seen) and a schematic of fabrication of a graphene/multi-walled CNT hybrid film (c).²⁵⁴ For steps 1–3, see text.

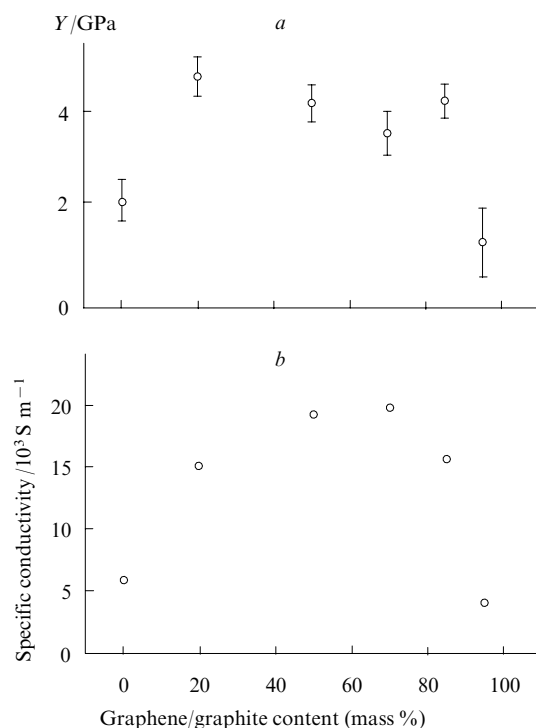


Figure 25. Young modulus (a) and specific conductivity (b) plotted vs. graphene content in composite.²⁵⁵

films was measured. The films prepared from pristine graphene appeared to be very brittle. The distribution of graphene in the mixtures was uniform. In most cases, graphene was aligned to the plane of the film (the exception is the specimen with 95% content of highly disordered graphene). The film prepared from pristine CNTs had a Young modulus of 2 GPa. The composites containing from 10% to 80% of graphene had much higher Young moduli (Fig. 25 a); however, the Young modulus of the specimen with a graphene content of 95% was equal to 1 GPa. A similar situation was observed for the specific conductivity, namely, it was equal to about $5.0 \times 10^3 \text{ S m}^{-1}$ for the film consisting of pristine CNTs, considerably increased with the graphene content, being equal to $20 \times 10^3 \text{ S m}^{-1}$ at a graphene content of 75%, and decreased to $3.0 \times 10^3 \text{ S m}^{-1}$ at a graphene content of 95% (see Fig. 25 a).

A solution-free method for preparation of composite films was proposed.²⁴⁷ Graphene–CNT films were grown separately in a reactor by chemical vapour phase deposition. Namely, the CNT film was deposited on nickel foil while graphene was fabricated on copper foil. Therefore, the sizes of both films were only limited to the size of the reactor. To attain better adhesion of CNTs, the graphene film was initially treated with ethanol, then dried and separated from the copper foil. The CNT film was separated from the substrate and transferred to graphene. The new film thus fabricated was multiply washed with deionized water. A scanning electron microscopy (SEM) study revealed that the film mainly consisted of single- and double-walled CNTs. A transparent, highly conductive composite was obtained.

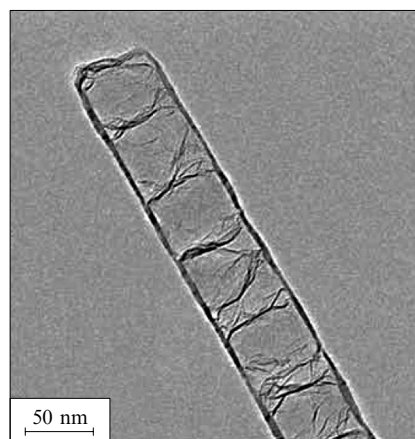


Figure 26. TEM image of individual CNT with graphene layers.²⁵⁶

Nanostructures comprising nitrogen-doped multi-walled CNTs with encapsulated graphene layers were reported (Fig. 26).²⁵⁶ Graphene layers were obtained *in situ* by chemical vapour phase deposition inside open-end CNTs ($\sim 50 \text{ nm}$ in diameter) grown vertically on a quartz substrate. Initially, graphene layers grew as fragments of the inner cavity of the multi-walled CNTs, but then detached from it at different sites and had different number of layers (from one to five). The authors of that study believed that graphene inside CNTs can act as additional electron conductor. Structures consisting of such nanotubes covered with metal nanoparticles are expected to be good catalysts because they have large surface areas, exhibit high electronic conductivity and are chemically stable. They can also be used for gas storage or energy conversion.

2. Theoretical research

a. The structure of composites

In 2008, a number of models for composites comprising only single-walled CNTs and single-layer graphene were proposed. Among them, there is a structure containing only sp^2 -hybridized atoms. It is produced by gradually ‘rolling’ a graphene sheet to a CNT through embedding six topological defects, namely, carbon heptagons.²⁴⁵ The attention of researchers was attracted to the following point: since graphene layers and CNTs can be prepared in solution, one can expect the formation of hybrid structures based on them with different energetically favourable configurations,²⁴⁶ because their ends are highly reactive.²³⁷ A structure consisting of a CNT attached through its open end to a graphene sheet (Fig. 27 a) and having $\text{C}(\text{sp}^3)$ atoms at the interface and structures obtained by reactive graphene edge attachment to the CNT surface (Fig. 27 b,c) were proposed. If a CNT is ‘capped’ or terminated with hydrogen atoms, graphene flakes are attracted to this CNT end through molecular forces and no covalent bonds are formed between them.²⁵⁷

Molecular ‘trapping’ of graphene fragments by the CNT surface was studied by the molecular dynamics method. It was proposed to prepare this type of molecular structures in a solution of a mixture of CNTs and graphene fragments.²⁵⁷ Helical wrapping of GNR around a CNT through van der Waals interaction at low temperatures was studied.^{260,261}

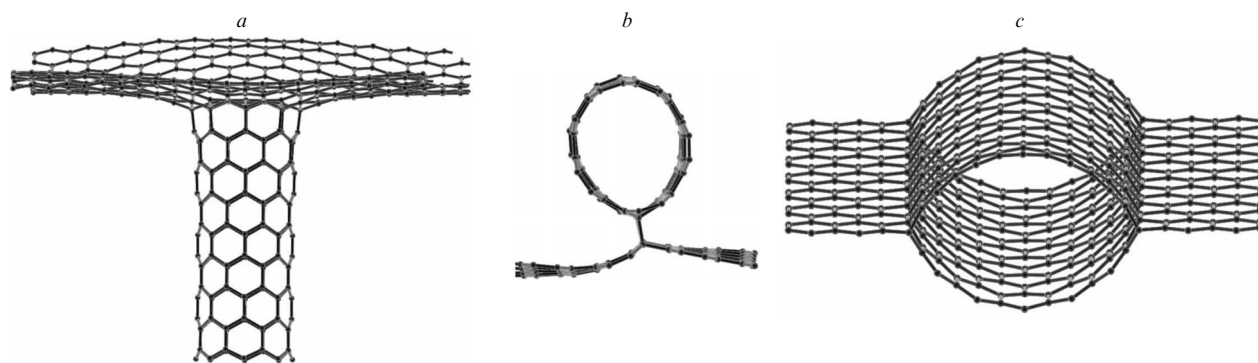


Figure 27. Models for composites: open-end attachment of a CNT to graphene surface (a), surface attachment of a CNT to graphene (b);²⁵⁷ and edge attachment of two graphene sheets to the CNT surface (c).^{246, 258, 259}

Structural models for the experimentally observed⁸⁹ encapsulation of GNR inside a CNT were constructed.^{260, 262}

The models considered here can serve to identify the synthesized structures and to assess the properties of the composites.

b. Properties of graphene–CNT structures

Studies on the electronic properties of graphene–CNT composite materials involved computer simulation of some configurations.

The electronic properties of a CNT attached by its lateral surface to edges of two graphene sheets were investigated.^{258, 259} The electronic spectrum of this structure can be represented by the sum of the electronic spectra of a graphene fragment and a distorted CNT. The spectrum of the latter resembles that of a CNT bearing hydrogen atoms attached to those CNT atoms to which graphene is attached (Fig. 28) and has little in common with the spectrum of a pristine CNT. This is due to the fact that chemisorption of graphene fragment leads to distortion of the atomic structure of the CNT. As can be seen, some van Hove peaks of the hybrid structure correspond to the CNT peaks, whereas other van Hove peaks correspond to graphene peaks. The peaks that are common to the composite and its constituents are denoted by vertical lines.

Analogous changes in the electronic spectrum follow attachment of two graphene fragments to the lateral surface of a CNT.²⁵⁹ The total spectrum of the composite is qualitatively described by the sum of the spectra of a GNR and an individual CNT distorted upon attachment of two ‘lines’ of hydrogen atoms. Attachment of graphene fragments to the CNT causes no loss of the conductivity of the composite.

The Young moduli of the CNTs bearing GNRs attached to the lateral surface increase with the number of GNRs.²⁵⁹ The calculated Young modulus of a CNT about 1 nm in diameter is 1.2–1.3 TPa, being close to the experimental value. Calculations predict the values $Y = 2.77, 2.83$ and 3.04 TPa for the structures bearing 2, 4 and 6 GNRs, respectively. In other words, the larger the number of the GNRs covalently bonded to the CNT the better the mechanical properties of the corresponding structures.

A structure prepared by patterned adsorption of small-diameter (5.5 Å) CNTs on graphene surface was studied.²⁶³ Its stable configuration is similar to the AB stacking in graphite, but the separation between the CNT and graphene

is 3.1–3.2 Å. The electronic spectrum of this structure depends strongly on the CNT diameter and can resemble the spectrum of a semimetal or a semiconductor (with a band gap less than 0.1 eV). However, this system is hard to

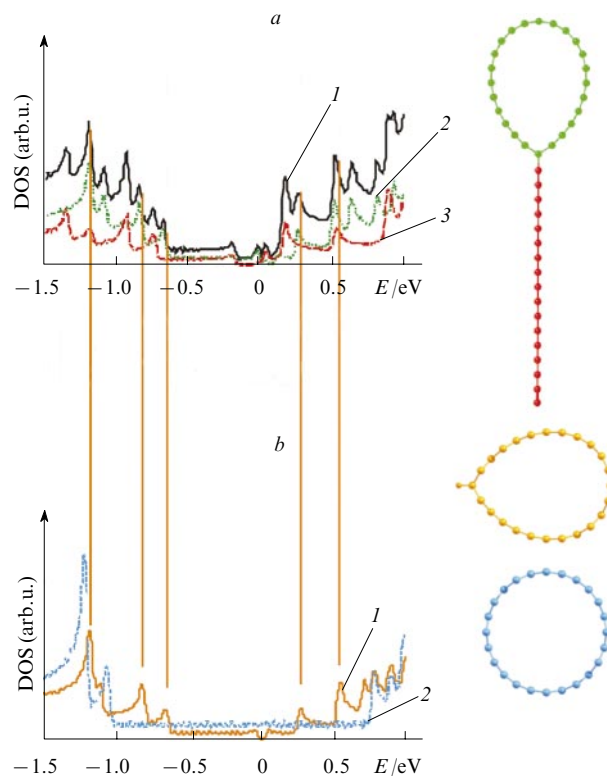


Figure 28. Density of states (DOS) for graphene–CNT composite.²⁵⁸

(a) Total density of electron states (1), partial density of states for CNT (2), partial density of states for graphene nanoribbon (3); shown on the right (from top to bottom) are projections of structures: CNT–graphene nanoribbon, a CNT with adsorbed ‘line’ of hydrogen atoms along the generatrix (shown is one H atom attached to the CNT) and pristine CNT.

(b) Density of electron states for pristine CNT (1) and the density of electron states for pristine CNT with a ‘line’ of hydrogen atoms (2). $E = 0$ is Fermi level.

synthesize because small-diameter CNTs are chemically unstable.

The interest in the structures comprising covalently bonded CNTs and fragments of graphene sheets²⁵⁹ did not cease more recently.^{264, 265} In particular, it was established²⁶⁴ that the energy gain from passivation of graphene edges by CNTs depends on the type of the CNTs ('armchair' CNT with attached 'zigzag'-type graphene edge is energetically the most favourable structure) and increases as the CNT diameter increases. Band gap oscillations were studied in detail²⁶⁵ for a GNR attached to different CNTs and it was found that the band gap values differ from one another depending on the CNT diameter.

The results of analysis of the electronic properties give grounds to hope for preparation of highly conductive materials from these hybrid nanostructures.

3. Applications of graphene–CNT composites

Graphene–CNT films exhibit good mechanical and conducting properties and can find applications in nano-²⁶⁶ and photoelectronics.²⁶⁷ Highly porous 'pillared graphene' can be utilized to produce elements for supercapacitors.^{268, 269}

Taking CNT,²⁷⁰ graphene,^{271, 272} GNRs²⁷³ and graphene²⁷⁴ as examples, it was shown that hydrogen uptake increases in the presence of alkali and alkaline-earth metal cations because they form chemical bonds with hydrogen atoms.^{275, 276} The results of computer simulation of the system 'pillared graphene' + adsorbed lithium cations indicate that the binding energy of hydrogen molecules and the total energy of the system increase by an order of magnitude in the presence of these cations and that the volumetric and gravimetric absorption also increase. The structure in question is suitable for integration into the metal–insulator–semiconductor complementary architecture.²⁶⁶

Polyaniline with small graphene and CNT additives was studied as material for supercapacitors;²⁶⁸ the additives increased the operating life and conductivity of the capacitors. Based on the results obtained, the composite was used as electrode material in vanadium redox flow batteries.²⁷⁷ To prepare the electrode, graphene and CNTs were mixed in different ratios (99 : 1, 97 : 3, 95 : 5, 93 : 7 and 91 : 9) and then dissolved in *N*-methyl-2-pyrrolidone along with 8% polyvinylidene fluoride. The mixture thus obtained was coated on platinum and dried at 30 °C for 12 h. This procedure was also used to prepare pristine CNT and graphene electrodes, which were used for comparison. Among the materials studied, the composite with a graphene:CNT ratio of 95 : 5 appeared to be the best candidate for electrode material.

An electrochemically stable layered structure analogous to 'pillared graphene' was proposed as electrode material for supercapacitors.²⁶⁹ It has a high specific capacitance (385 F g⁻¹) which increases by 20% after 2000 charge–discharge cycles.

Graphene–CNT films²⁶⁷ are characterized by high electrochemical stability. Carbon nanotubes were synthesized by catalytic decomposition of propylene on Fe/Al₂O₃ catalyst, purified and cut in a H₂SO₄ + HNO₃ solution at 140 °C. Then, the CNTs were filtered, washed with deionized water and dispersed in a suspension of nanographite. The suspension was prepared from graphite oxide by the Hummers method, dissolved in water and dialyzed to completely remove salt and oxide residues. The suspension

was allowed to stay in a quartz reactor for 1 h (750 °C, argon atmosphere). Then, H₂ (100 cm³ min⁻¹) and CO₂ (70 cm³ min⁻¹) were supplied into the reactor at the same temperature. As a result, a 'sandwich' was formed, consisting of graphene sheets and CNTs nonuniformly distributed around the periphery of the graphene sheets. According to TEM data, most CNTs were multi-walled and had lengths to 100 nm long and outer diameters from 7 to 12 nm. The same experiment was carried out with other gaseous sources of carbon; it was shown that changes in the chemical compositions of the gases and in their concentrations cause the CNT morphology to change. When using methane, the CNT length reached 1–2 μm; in the case of carbon oxide, shorter CNTs were grown.

Since high-quality graphene can be obtained and transferred to a bundle of single-walled CNTs, which generate electron–hole pairs better than multi-walled CNTs, it is possible to fabricate a material for elements of new-generation solar cells with better properties compared to those of the CNT bundles.²⁶⁷

A model for a hybrid solar cell with a heterojunction at the TiO₂ (or CdSe) quantum dots/graphene interface is schematically shown in Fig. 29. In this composite, graphene can be used as transparent conductive electrode and CNTs can not only act as good electron or hole conductors, but also separate them. These materials are promising for the design of elements for new-generation, carbon-only solar cells (TiO₂ or CdSe quantum dots are replaced by C₆₀ fullerene layers). The first publication on the design of a solar cell with main components made of carbon materials is available.²⁷⁸ A bilayer polymer consisting of pre-selected semiconductor single-walled CNTs was used as ultrathin anode, a layer of fullerenes with scandium nanoparticles was used as the active medium and a layer of graphene flakes played the role of cathode.

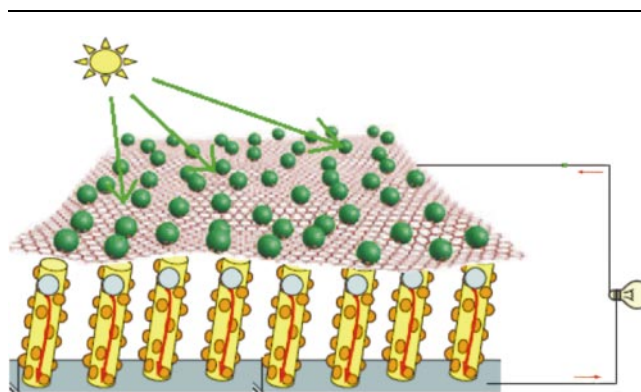


Figure 29. Schematic of a hybrid solar cell (<http://phys570x.wikispaces.com/file/view/Proposal+write-up.pdf>).

Graphene is covered with TiO₂ (or CdSe) quantum dots. Exposure to light causes generation of electron–hole pairs.

V. Conclusion

In this review we generalized the results of studies on GNRs and graphene structures that were either modified with hydrogen and fluorine or treated as constituents of carbon composites. These results were left out of consideration or only briefly outlined earlier. For instance, we noted that

many theoretical models were proposed for functionalized graphene structures but only a few of them were confirmed experimentally. The reverse situation is also possible, namely, there are some publications on the preparation of pure carbon composites by mixing graphene fragments and CNTs, but none of them includes an analysis of the type of the bond between the constituents and presents structural models for compounds. These examples point to the need to bridge the gap between experiment and theory in the research on the synthesis and properties of novel materials.

Currently, technologies for fabrication of these structures and for the design of devices based on them are improved using novel physicochemical methods. Consider one of them as an example. There is a cheap and efficient procedure for fluorination of graphene to controlled C:F ratio by the reaction of dispersed graphene oxide with hydrofluoric acid in aqueous solution.²⁷⁹ Fluorine atoms are adsorbed on the basal plane of graphene. The C:F ratio can be varied with ease by varying reaction conditions. This makes it possible to prepare fluorinated single-layer of bilayer graphene with band gaps from 1.82 to 2.99 eV. The material may find application in optoelectronics and in photonics devices.

Not only pure graphene structures, but also structures based on graphene oxide attract the attention of researchers. For instance, by coating a titanium substrate with aqueous dispersion of CNTs and graphene oxide one can obtain 3D structures comprising CNTs (usually, 12.5 mass %) penetrating graphene oxide layers; these structures formed in the course of annealing by self-assembly.²⁸⁰ Supercapacitors fabricated using these films exhibit excellent electrochemical properties, namely, a high specific capacitance of 428 and 145 F at a current density of 0.5 and 100 A g⁻¹, respectively, and a retention rate of 98% of the initial capacitance after 10 000 charge–discharge cycles.

Hydrophilic graphene oxide was transformed to hydrophobic graphene oxide by fluorination.²⁸¹ The method for preparation of graphene-based surfaces with tunable wettability is very simple and opens the way to cheap hydrophobic coatings. This allows one to prepare paints that can be sputtered on various porous and nonporous surfaces.

Graphene nanoribbons and nanostrips on modified graphene, in which the electron mobility is much higher than in the same-size silicon structures, represent a new class of promising semiconductor materials whose electrical and optical properties are more attractive than those of silicon devices. In the future, conventional silicon transistors will be replaced by the new-generation materials.

For instance, fabrication of the first top-gated graphene transistor²⁸² was followed by significant improvement of the efficiency of high-frequency graphene-based transistors. At present, graphene transistors have a cut-off frequency of 300 and 420 GHz at gate lengths of 140 and 67 nm, respectively.²⁸³ Owing to high mobility of electrons in graphene these frequencies are much higher than those of silicon transistors (140 and 250 GHz), being comparable with the frequencies of the best A^{III}/B^V semiconductor transistors (300–400 GHz) at similar gate lengths. The possibility for graphene transistors with gate lengths from 9.86 to 0.91 nm to operate in the frequency range from 3.4 to 21.0 THz was substantiated theoretically.²⁸⁴

Not only graphene transistors, but also different kinds of integrated circuits including nonlinear mixers, voltage amplifiers and inverters have been implemented.²⁸³ This can

be treated as considerable progress despite the fact that graphene electronics is still in the early stage.

Summing up, graphene-based materials considered in this review exhibit a variety of physicochemical properties that offer great prospects for various scientific and engineering applications.²⁸⁵

Novel 2D analogues of graphene also attract considerable attention of researchers.⁸ This is confirmed by the fact that the initiative in description and systematization of research on graphene-like 2D materials proposed by Ivanovskii¹⁶ was recently taken up by Xu *et al.*²⁸⁶

This review has been written with the financial support from the Russian Foundation for Basic Research (Project Nos 11-02-01453-a and 12-02-31261) and the F7-2012 Programme (Project FP7-318617 FAEMCAR) and the Ministry of Education and Science of the Russian Federation (Federal Contract No. 14.B37.21.1645).

References

1. A H C Neto, F Guinea, N M R Peres, K S Novoselov, A K Geim *Rev. Mod. Phys.* **81** 109 (2009)
2. D A Bochvar, E G Gal'pern *Proc. Acad. Sci. USSR* **209** 239 (1973) [*Dokl. Akad. Nauk SSSR* **209** 610 (1973)]
3. J H Weaver, J L Martins, T Komeda, Y Chen, T R Ohno, G H Kroll, N Troullier, R E Haufler, R E Smalley *Phys. Rev. Lett.* **66** 1741 (1991)
4. D T W Ebbesen, D H Hiura *Adv. Mater.* **7** 582 (1995)
5. X Lu, M Yu, H Huang, R S Ruoff *Nanotechnology* **10** 269 (1999)
6. E Dujardin, T Thio, H Lezec, T W Ebbesen *Appl. Phys. Lett.* **79** 2474 (2001)
7. Y Gan, W Chu, L Qiao *J. Phys. Soc. Jpn.* **539** 120 (2003)
8. K S Novoselov, D Jiang, F Schedin, T J Booth, V V Khotkevich, S V Morozov, A K Geim *Proc. Natl. Acad. Sci. USA* **102** 10451 (2005)
9. A K Geim *Phys. Scr.* 014003 (2012)
10. D W Boukhvalov, M I Katsnelson *J. Phys.: Condens. Matter* **21** 344205 (2009)
11. J K Wassei, R B Kaner *Mater. Today* **13** 52 (2010)
12. A Y Kryukov, S Y Davydov, I M Izvol'skii, E G Rakov, N V Abramova, V I Sokolov *Mendeleev Commun.* **22** 237 (2012)
13. E D Grayfer, V G Makotchenko, A S Nazarov, S J Kim, V E Fedorov *Russ. Chem. Rev.* **80** 751 (2011)
14. A V Elets'kii, I M Iskandarova, A A Knizhnik, D N Krasikov *Physics-Uspekhi* **54** 227 (2011) [*Usp. Fiz. Nauk* **181** 233 (2011)]
15. P B Sorokin, L A Chernozatonskii *Physics-Uspekhi* **56** 105 (2013) [*Usp. Fiz. Nauk* **183** 113 (2013)]
16. A L Ivanovskii *Russ. Chem. Rev.* **81** 571 (2012)
17. M Katsnelson *Science* **329** 1157 (2010)
18. S V Morozov, K S Novoselov, A K Geim *Physics-Uspekhi* **51** 744 (2008); [*Usp. Fiz. Nauk* **178** 776 (2008)]
19. J C Meyer, A K Geim, M I Katsnelson, K S Novoselov, T J Booth, S Roth *Nature (London)* **446** 60 (2007)
20. M I Katsnelson, K S Novoselov, A K Geim *Nat. Phys.* **2** 620 (2006)
21. N Stander, B Huard, D Goldhaber-Gordon *Phys. Rev. Lett.* **102** 026807 (2009)
22. M I Katsnelson *Eur. Phys. J., B* **51** 157 (2006)
23. K S Novoselov *Rev. Mod. Phys.* **83** 837 (2011)

24. K S Novoselov, A K Geim, S V Morozov, D Jiang, M I Katsnelson, I V Grigorieva, S V Dubonos, A A Firsov *Nature (London)* **438** 197 (2005)
25. S Bae, H Kim, Y Lee, X Xu, J S Park, Y Zheng, J Balakrishnan, T Lei, H R Kim, Y I Song, Y J Kim, K S Kim, B Özyilmaz, J H Ahn, B H Hong, S Iijima *Nat. Nanotechnol.* **5** 574 (2010)
26. K S Novoselov, A K Geim, S V Morozov, D Jiang, Y Zhang, S V Dubonos, I V Grigorieva, A A Firsov *Science* **306** 666 (2004)
27. P Blake, P D Brimicombe, R R Nair, T J Booth, D Jiang, F Schedin, L A Ponomarenko, S V Morozov, H F Gleeson, E W Hill, A K Geim, K S Novoselov *Nano Lett.* **8** 1704 (2008)
28. R Chau, B Doyle, S Datta, J Kavalieros, K Zhang *Nat. Mater.* **6** 810 (2007)
29. Y Wu, Y M Lin, A A Bol, K A Jenkins, F Xia, D B Farmer, Y Zhu, P Avouris *Nature (London)* **472** 74 (2011)
30. M Sprinkle, M Ruan, Y Hu, J Hankinson, M Rubio-Roy, B Zhang, X Wu, C Berger, W A de Heer *Nat. Nanotechnol.* **5** 727 (2010)
31. A B Kuzmenko, E V Heumen, F Carbone, D van der Marel *Phys. Rev. Lett.* **100** 117401 (2008)
32. C M Weber, D M Eisele, J P Rabe, Y Liang, X Feng, L Zhi, K Müllen, J L Lyon, R Williams, D A V Bout, K J Stevenson *Small* **6** 184 (2010)
33. R R Nair, P Blake, A N Grigorenko, K S Novoselov, T Booth, T Stauber, N M R Peres, A K Geim *Science* **320** 1308 (2008)
34. C Casiraghi, A Hartschuh, E Lidorikis, H Qian, H Harutyunyan, T Gokus, K S Novoselov, A C Ferrari *Nano Lett.* **7** 2711 (2007)
35. Y Zhu, Z Sun, Z Yan, Z Jin, J M Tour *ACS Nano* **5** 6472 (2011)
36. L G D Arco, Y Zhang, C W Schlenker, K Ryu, M E Thompson, C Zhou *ACS Nano* **4** 2865 (2010)
37. F Xia, T Mueller, Y M Lin, A Valdes-Garcia, P Avouris *Nat. Nanotechnol.* **4** 839 (2009)
38. T J Echtermeyer, L Britnell, P K Jasnós, A Lombardo, R V Gorbachev, A N Grigorenko, A K Geim, A C Ferrari, K S Novoselov *Nat. Commun.* **2** 458 (2011)
39. M D Stoller, S Park, Y Zhu, J An, R S Ruoff *Nano Lett.* **8** 3498 (2008)
40. M F El-Kady, V Strong, S Dubin, R B Kaner *Science* **335** 1326 (2012)
41. K S Novoselov, V I Fal'ko, L Colombo, P R Gellert, M G Schwab, K Kim *Nature (London)* **490** 192 (2012)
42. C Lee, X Wei, J Kysar, J Hone *Science* **321** 385 (2008)
43. D Wei, Y Liu *Adv. Mater.* **22** 3225 (2010)
44. M Fujita, K Wakabayashi, K Nakada, K Kusakabe *J. Phys. Soc. Jpn.* **65** 1920 (1996)
45. K Nakada, M Fujita, G Dresselhaus, M S Dresselhaus *Phys. Rev. B* **54** 17954 (1996)
46. V H O Barone, G E Scuseria *Nano Lett.* **6** 2748 (2006)
47. Y W Son, M L Cohen, S G Louie *Nature (London)* **444** 347 (2006)
48. Y W Son, M L Cohen, S G Louie *Phys. Rev. Lett.* **97** 216803 (2006)
49. R Saito, G Dresselhaus, M S Dresselhaus, in *Physical Properties of Carbon Nanotubes* (London: Imperial College Press, 1998) p. 259
50. L A Chernozatonskii, P B Sorokin, J W Brüning *Appl. Phys. Lett.* **91** 183103 (2007)
51. A K Singh, B I Yakobson *Nano Lett.* **9** 1540 (2009)
52. M A Ribas, A K Singh, P B Sorokin, B I Yakobson *Nano Res.* **4** 143 (2011)
53. H Lee, Y W Son, N Park, S Han, J Yu *Phys. Rev. B* **72** 174431 (2005)
54. F Cervantes-Sodi, G Csúnyi, S Piscanec, A C Ferrari *Phys. Rev. B* **77** 165427 (2008)
55. K A Ritter, J W Lyding *Nat. Mater.* **8** 235 (2009)
56. Z F Wang, Q Li, H Zheng, H Ren, H Su, Q W Shi, J Chen *Phys. Rev. B* **75** 113406 (2007)
57. A P Seitsonen, A M Saitta, T Wassmann, M Lazzeri, F Mauri *Phys. Rev. B* **82** 115425 (2010)
58. P Koskinen, S Malola, H Hókkinen *Phys. Rev. Lett.* **101** 115502 (2008)
59. P Koskinen, S Malola, H Hókkinen *Phys. Rev. B* **80** 73401 (2009)
60. V I Artyukhov, Y Liu, B I Yakobson *Proc. Natl. Acad. Sci. USA* **109** 15136 (2012)
61. J Gao, J Zhao, F Ding *J. Am. Chem. Soc.* **134** 6204 (2012)
62. X Li, X Wang, L Zhang, S Lee, H Dai *Science* **319** 1229 (2008)
63. C Tao, L Jiao, O V Yazyev, Y C Chen, J Feng, X Zhang, R B Capaz, J M Tour, A Zettl, S G Louie, H Dai, M F Crommie *Nat. Phys.* **7** 616 (2011)
64. L Tapasztó, G Dobrik, P Lambin, L P Biró *Nat. Nanotechnol.* **3** 397 (2008)
65. P Ruffieux, J Cai, N C Plumb, L Patthey, D Prezzi, A Ferretti, E Molinari, X Feng, K Müllen, C A Pignedoli, R Fasel *ACS Nano* **6** 6930 (2012)
66. X Liang, Y S Jung, S Wu, A Ismach, D L Olynick, S Cabrini, J Bokor *Nano Lett.* **10** 2454 (2010)
67. S Linden, D Zhong, A Timmer, N Aghdassi, J H Franke, H Zhang, X Feng, K Müllen, H Fuchs, L Chi, H Zacharias *Phys. Rev. Lett.* **108** 216801 (2012)
68. J Bai, X Duan, Y Huang *Nano Lett.* **9** 2083 (2009)
69. A C Simonsen, H G N Rubahn *Nano Lett.* **2** 1379 (2002)
70. X Wang, Y Ouyang, L Jiao, H Wang, L Xie, J Wu, J Guo, H Dai *Nat. Nanotechnol.* **6** 563 (2011)
71. R Mondal, B K Shah, D C Neckers *J. Am. Chem. Soc.* **128** 9612 (2006)
72. F Börrnert, L Fu, S Gorantla, M Knupfer, B Büchner, M H Rummeli *ACS Nano* **6** 10327 (2012)
73. G Liu, Y Wu, Y M Lin, D B Farmer, J A Ott, J Bruley, A Grill, P Avouris, D Pfeiffer, A A Balandin, C Dimitrakopoulos *ACS Nano* **6** 6786 (2012)
74. L Jiao, L Xie, H Dai *Nano Res.* **5** 292 (2012)
75. J Bai, X Zhong, S Jiang, Y Huang, X Duan *Nat. Nanotechnol.* **5** 190 (2010)
76. X Wang, H Dai *Nat. Chem.* **2** 661 (2010)
77. A L Elias, A R Botello-Méndez, D Meneses-Rodríguez, V J Gonzalez, D Ramirez-González, L Ci, E Munoz-Sandoval, P M Ajayan, H Terrones, M Terrones *Nano Lett.* **10** 366 (2009)
78. H R Gutiérrez, U J Kim, J P Kim, P C Eklund *Nano Lett.* **5** 2195 (2005)
79. M Zhang, D H Wu, C L Xu, Y F Xu, W K Wang *Nanostruct. Mater.* **10** 1145 (1998)
80. A G Cano-Marquez, F J Rodriguez-Macias, J Campos-Delgado, C G Espinosa-Gonzalez, F Tristan-Lopez, D Ramirez-Gonzalez, D A Cullen, D J Smith, M Terrones, Y I Vega-Cant *Nano Lett.* **9** 1527 (2009)
81. D V Kosynkin, A L Higginbotham, A Sinitskii, J R Lomeda, A Dimiev, B K Price, J M Tour *Nature (London)* **458** 872 (2009)

82. A L Higginbotham, D V Kosynkin, A Sinit'skii, Z Sun, J M Tour *ACS Nano* **4** 2059 (2010)
83. D V Kosynkin, W Lu, A Sinit'skii, G Pera, Z Sun, J M Tour *ACS Nano* **5** 968 (2011)
84. A V Talyzin, S Luzan, I V Anoshkin, A G Nasibulin, H Jiang, E I Kauppinen, V M Mikoushkin, V V Shnitov, D E Marchenko, D Noreus *ACS Nano* **5** 5132 (2011)
85. L Jiao, X Wang, G Diankov, H Wang, H Dai *Nat. Nanotechnol.* **5** 321 (2010)
86. L Jiao, L Zhang, X Wang, G Diankov, H Dai *Nature (London)* **458** 877 (2009)
87. L Jiao, L Zhang, L Ding, J Liu, H Dai *Nano Res.* **3** 387 (2010)
88. J Cai, P Ruffieux, R Jaafar, M Bieri, T Braun, S Blankenburg, M Muoth, A P Seitsonen, M Saleh, X Feng, K Müllen, R Fasel *Nature (London)* **466** 470 (2010)
89. A V Talyzin, I V Anoshkin, A V Krashenninikov, R M Nieminen, A G Nasibulin, H Jiang, E I Kauppinen *Nano Lett.* **11** 4352 (2011)
90. A Chuvilin, E Bichoutskaia, M C Gimenez-Lopez, T W Chamberlain, G A Rance, N Kuganathan, J Biskupek, U Kaiser, A N Khlobystov *Nat. Mater.* **10** 687 (2011)
91. P Kovacic, A Kyriakis *J. Am. Chem. Soc.* **85** 454 (1963)
92. W J Bailey, C W Liao *J. Am. Chem. Soc.* **77** 992 (1955)
93. L P Biró, L Hevesi, P Lambin *Nanopages* **5** 1 (2010)
94. M Murakami, S Iijima, Y Susumu *J. Appl. Phys.* **60** 3856 (1986)
95. R R Nair, W Ren, R Jalil, I Riaz, V G Kravets, L Britnell, P Blake, F Schedin, A S Mayorov, S Yuan, M I Katsnelson, H M Cheng, W Strupinski, L G Bulusheva, A V Okotrub, I V Grigorieva, A N Grigorenko, K S Novoselov, A K Geim *Small* **6** 2877 (2010)
96. Y Shao, J Wang, H Wu, J Liu, I Aksay, Y Lin *Electroanalysis* **22** 1027 (2010)
97. T Kuilaa, S Bosea, A K Mishrab, P Khanraa, N H Kimc, J H Leeabc *Prog. Mater. Sci.* **57** 1061 (2012)
98. L Yan, Y B Zheng, F Zhao, S Li, X Gao, B Xu, P S Weiss, Y Zhao *Chem. Soc. Rev.* **41** 97 (2011)
99. I V Zaporot'skova, A O Litinskii, L A Chernozatonskii *J. Exp. Theor. Phys. Lett.* **66** 841 (1997) [*Pis'ma Zh. Eksp. Teor. Fiz.* **66** 799 (1997)]
100. T Y Astakhova, G A Vinogradov, O D Gurin, M Menon *Russ. Chem. Bull., Eng. Transl.* **51** 764 (2002) [*Izv. Akad. Nauk, Ser. Khim.* 704 (2002)]
101. P Ruffieux, O Grining, M Biemann, P Mauron, L Schlapbach, P Grining *Phys. Rev. B* **66** 245416 (2002)
102. M H F Sluiter, Y Kawazoe *Phys. Rev. B* **68** 085410 (2003)
103. J O Sofo, A S Chaudhari, G D Barber *Phys. Rev. B* **75** 153401 (2007)
104. O Leenaerts, H Peelaers, A D Hernández-Nieves, B Partoens, F M Peeters *Phys. Rev. B* **82** 195436 (2010)
105. V I Artyukhov, L A Chernozatonskii *J. Phys. Chem. A* **114** 5389 (2010)
106. A Bhattacharya, S Bhattacharya, C Majumder, G P Das *Phys. Rev. B* **83** 033404 (2011)
107. D C Elias, R R Nair, T M G Mohiuddin, S V Morozov, P Blake, M P Halsall, A C Ferrari, D W Boukhvalov, M I Katsnelson, A K Geim *Science* **323** 610 (2009)
108. Z Luo, T Yu, K Kim, Z Ni, Y You, S Lim, Z Shen, S Wang, J Lin *ACS Nano* **3** 1781 (2009)
109. Y Lin, F Ding, B I Yakobson *Phys. Rev. B* **78** 041402(R) (2008)
110. M Z S Flores, P A S Autreto, S B Legoas, D S Galvao *Nanotechnology* **20** 465704 (2009)
111. H Gao, L Wang, J Zhao, F Ding, L Jianping *J. Phys. Chem. C* **115** 3236 (2011)
112. L A Chernozatonskii, D G Kvashnin, P B Sorokin, A G Kvashnin, J Brüning *J. Phys. Chem. C* **116** 20035 (2012)
113. E J Duplock, M Scheffler, P J D Lindan *Phys. Rev. Lett.* **92** 225502 (2004)
114. L A Chernozatonskii, P B Sorokin, E É Belova, J Brüning, A S Fedorov *J. Exp. Theor. Phys. Lett.* **85** 77 (2007) [*Pis'ma Zh. Eksp. Teor. Fiz.* **85** 84 (2007)]
115. L Hornekr, Ž Šljivančanin, W Xu, R Otero, E Rauls, I Stensgaard, E Lægsgaard, B Hammer, F Besenbacher *Phys. Rev. Lett.* **96** 156104 (2006)
116. L A Chernozatonskii, P B Sorokin *J. Phys. Chem. C* **114** 3225 (2010)
117. L Nilsson, Ž Šljivančanin, R Balog, W Xu, T Linderöth, E Lægsgaard, I Stensgaard, B Hammer, F Besenbacher, L Hornekr *Carbon* **50** 2052 (2012)
118. L A Chernozatonskii, P B Sorokin *Phys. Status Solidi, B* **245** 2086 (2008)
119. L A Chernozatonskii, A A Artyukh, D G Kvashnin *J. Exp. Theor. Phys. Lett.* **95** 266 (2012) [*Pis'ma Zh. Eksp. Teor. Fiz.* **95** 290 (2012)]
120. P Sessi, J R Guest, M Bode, N P Guisinger *Nano Lett.* **9** 4343 (2009)
121. H Zhang, Y Miyamoto, A Rubio *Phys. Rev. B* **85** 201409(R) (2012)
122. R Balog, B Jørgensen, L Nilsson, M Andersen, E Rienks, M Bianchi, M Fanetti, E Lægsgaard, A Baraldi, S Lizzit, Z Šljivančanin, F Besenbacher, B Hammer, T G Pedersen, P Hofmann, L Hornekr *Nat. Mater.* **9** 315 (2010)
123. S Ryu, M Y Han, J Maultzsch, T F Heinz, P Kim, M L Steigerwald, L E Brus *Nano Lett.* **8** 4597 (2008)
124. Z Sun, C L Pint, D C Marcano, C Zhang, J Yao, G Ruan, Z Yan, Y Zhu, R H Hauge, J M Tour *Nat. Commun.* **2** 559 (2011)
125. J Kim, L J Cote, F Kim, J Huang *J. Am. Chem. Soc.* **132** 260 (2009)
126. L A Openov, A I Podlivaev *J. Exp. Theor. Phys. Lett.* **90** 459 (2009) [*Pis'ma Zh. Eksp. Teor. Fiz.* **90** 505 (2009)]
127. L F Huang, X H Zheng, G R Zhang, L L Li, Z Zeng *J. Phys. Chem. C* **115** 21088 (2011)
128. Z M Ao, A D Hernández-Nieves, F M Peeters, S Li *Appl. Phys. Lett.* **97** 233109 (2010)
129. Y Li, Z Zhou, P Shen, Z Chen *J. Phys. Chem. C* **113** 15043 (2009)
130. H Sahin, C Ataca, S Ciraci *Phys. Rev. B* **81** 205417 (2010)
131. Y H Lu, Y P Feng *J. Phys. Chem. C* **113** 20841 (2009)
132. Y Kita, N Watanabe, Y Fujii *J. Am. Chem. Soc.* **101** 3832 (1979)
133. J T Robinson, J S Burgess, C E Junkermeier, S C Badescu, T L Reinecke, F K Perkins, M K Zalalutdinov, J W Baldwin, J C Culbertson, P E Sheehan, E S Snow *Nano Lett.* **10** 3001 (2010)
134. H Touhara, K Kadono, Y Fujii, N Watanabe *Z. Anorg. Allg. Chem.* **544** 7 (1987)
135. N Watanabe *Solid State Ionics* **1** 87 (1980)
136. K N Kudin, G E Scuseria, B I Yakobson *Phys. Rev. B* **64** 235406 (2001)
137. K N Kudin, H F Bettinger, G E Scuseria *Phys. Rev. B* **63** 045413 (2001)
138. S H Cheng, K Zou, F Okino, H R Gutierrez, A Gupta, N Shen, P C Eklund, J O Sofo, J Zhu *Phys. Rev. B* **81** 205435 (2010)

139. R Zbořil, F Karlický, A B Bourlino, T A Steriotis, A K Stubos, V Georgakilas, K Šafářová, D Jančík, C Trapalis, M Otyepka *Small* **6** 2885 (2010)
140. K J Jeon, Z Lee, E Pollak, L Moreschini, A Bostwick, C M Park, R Mendelsberg, V Radmilovic, R Kostecki, T J Richardson, E Rotenberg *ACS Nano* **5** 1042 (2011)
141. A B Bourlino, K Safarova, K Siskova, R Zbořil *Carbon* **50** 1425 (2012)
142. F Withers, M Dubois, A K Savchenko *Phys. Rev. B* **82** 073403 (2010)
143. D K Samarakoon, Z Chen, C Nicolas, X Q Wang *Small* **7** 965 (2011)
144. E Muñoz, A K Singh, M A Ribas, E S Penev, B I Yakobson *Diam. Relat. Mater.* **19** 368 (2010)
145. J C Charlier, X Gonze, J P Michenaud *Phys. Rev. B* **47** 16162 (1993)
146. Y Takagi, K Kusakabe *Phys. Rev. B* **65** 121103 (2002)
147. F Withers, T H Bointon, M Dubois, S Russo, M F Craciun *Nano Lett.* **11** 3912 (2011)
148. D R Dreyer, S Park, C W Bielawski, R S Ruoff *Chem. Soc. Rev.* **39** 228 (2009)
149. D A Stewart, K A Mkhoyan, in *Graphene Nanoelectronics: Metrology, Synthesis, Properties and Applications* (Ed. H Raza) (Berlin, Heidelberg: Springer, 2012) p. 435
150. S Mao, H Pu, J Chen *RSC Adv.* **2** 2643 (2012)
151. B C Brodie *Philos. Trans. R. Soc. London* **149** 249 (1859)
152. L Staudenmaier *Ber. Dtsch. Chem. Ges.* **31** 1481 (1898)
153. W S Hummers Jr, R E Offeman *J. Am. Chem. Soc.* **80** 1339 (1958)
154. U Hofmann, R Holst *Ber. Dtsch. Chem. Ges.* **72** 754 (1939)
155. G Ruess *Monatsh. Chem.* **76** 381 (1947)
156. W Scholz, H P Boehm *Z. Anorg. Allg. Chem.* **369** 327 (1969)
157. T Nakajima, A Mabuchi, R Hagiwara *Carbon* **26** 357 (1988)
158. A Lerf, H He, M Forster, J Klinowski *J. Phys. Chem. B* **102** 4477 (1998)
159. T Szabó, O Berkesi, P Forgó, K Josepovits, Y Sanakis, D Petridis, I Dékány *Chem. Mater.* **18** 2740 (2006)
160. D Pandey, R Reifengerger, R Piner *Surf. Sci.* **602** 1607 (2008)
161. H K Jeong, M H Jin, K P So, S C Lim, Y H Lee *J. Phys. D: Appl. Phys.* **42** 065418 (2009)
162. Z Luo, P M Vora, E J Mele, A T C Johnson, J M Kikkawa *Appl. Phys. Lett.* **94** 111909 (2009)
163. G Eda, Y Y Lin, C Mattevi, H Yamaguchi, H A Chen, I S Chen, C W Chen, M Chhowalla *Adv. Mater.* **22** 505 (2010)
164. D W Boukhvalov, M I Katsnelson *J. Am. Chem. Soc.* **130** 10697 (2008)
165. J Ito, J Nakamura, A Natori *J. Appl. Phys.* **103** 113712 (2008)
166. J A Yan, L Xian, M Y Chou *Phys. Rev. Lett.* **103** 086802 (2009)
167. S Stankovich, D A Dikin, R D Piner, K A Kohlhaas, A Kleinhammes, Y Jia, Y Wu, S T Nguyen, R S Ruoff *Carbon* **45** 1558 (2007)
168. H Chen, M B Müller, K J Gilmore, G G Wallace, D Li *Adv. Mater.* **20** 3557 (2008)
169. S Park, J An, I Jung, R D Piner, S J An, X Li, A Velamakanni, R S Ruoff *Nano Lett.* **9** 1593 (2009)
170. V C Tung, M J Allen, Y Yang, R B Kaner *Nat. Nanotechnol.* **4** 25 (2009)
171. D Li, M B Müller, S Gilje, R B Kaner, G G Wallace *Nat. Nanotechnol.* **3** 101 (2008)
172. H Wang, J T Robinson, X Li, H Dai *J. Am. Chem. Soc.* **131** 9910 (2009)
173. Y Xu, H Bai, G Lu, C Li, G Shi *J. Am. Chem. Soc.* **130** 5856 (2008)
174. C Y Su, Y Xu, W Zhang, J Zhao, A Liu, X Tang, C H Tsai, Y Huang, L J Li *ACS Nano* **4** 5285 (2010)
175. D R Dreyer, S Murali, Y Zhu, R S Ruoff, C W Bielawski *J. Mater. Chem.* **21** 3443 (2011)
176. Y Si, E T Samulski *Nano Lett.* **8** 1679 (2008)
177. W Gao, L B Alemany, L Ci, P M Ajayan *Nat. Chem.* **1** 403 (2009)
178. H J Shin, K K Kim, A Benayad, S M Yoon, H K Park, I S Jung, M H Jin, H K Jeong, J M Kim, J Y Choi, Y H Lee *Adv. Funct. Mater.* **19** 1987 (2009)
179. R Wang, J Sun, L Gao, C Xu, J Zhang, Y Liu *Nanoscale* **3** 904 (2011)
180. S Pei, J Zhao, J Du, W Ren, H M Cheng *Carbon* **48** 4466 (2010)
181. I K Moon, J Lee, R S Ruoff, H Lee *Nat. Commun.* **1** 73 (2010)
182. X Fan, W Peng, Y Li, X Li, S Wang, G Zhang, F Zhang *Adv. Mater.* **20** 4490 (2008)
183. S Park, J An, R D Piner, I Jung, D Yang, A Velamakanni, S T Nguyen, R S Ruoff *Chem. Mater.* **20** 6592 (2008)
184. Z J Fan, W Kai, J Yan, T Wei, L J Zhi, J Feng, Y M Ren, L P Song, F Wei *ACS Nano* **5** 191 (2010)
185. Z Fan, K Wang, T Wei, J Yan, L Song, B Shao *Carbon* **48** 1686 (2010)
186. X Li, H Wang, J T Robinson, H Sanchez, D Georgi, H Dai *J. Am. Chem. Soc.* **131** 15939 (2009)
187. D Long, W Li, L Ling, J Miyawaki, I Mochida, S H Yoon *Langmuir* **26** 16096 (2010)
188. O C Compton, D A Dikin, K W Putz, L C Brinson, S T Nguyen *Adv. Mater.* **22** 892 (2010)
189. W Chen, L Yan, P R Bangal *J. Phys. Chem. C* **114** 19885 (2010)
190. T Zhou, F Chen, K Liu, H Deng, Q Zhang, J Feng, Q Fu *Nanotechnology* **22** 045704 (2011)
191. S Mao, K Yu, S Cui, Z Bo, G Lu, J Chen *Nanoscale* **3** 2849 (2011)
192. S Wakelanda, R Martineza, J K Greyb, C C Luhrs *Carbon* **48** 3463 (2010)
193. F Yang, Y Liu, L Gao, J Sun *J. Phys. Chem. C* **114** 22085 (2010)
194. M J Fernandez-Merino, L Guardia, J I Paredes, S Villar-Rodil, P Solis-Fernandez, A Martinez-Alonso, J M D Tascon *J. Phys. Chem. C* **114** 6426 (2010)
195. S Dubin, S Gilje, K Wang, V C Tung, K Cha, A S Hall, J Farrar, R Varshneya, Y Yang, R B Kaner *ACS Nano* **4** 3845 (2010)
196. S M Kang, S Park, D Kim, S Y Park, R S Ruoff, H Lee *Adv. Funct. Mater.* **21** 108 (2011)
197. J Liu, S Fu, B Yuan, Y Li, Z Deng *J. Am. Chem. Soc.* **132** 7279 (2010)
198. G Williams, B Seger, P V Kamat *ACS Nano* **2** 1487 (2008)
199. O Akhavan, M Abdolhad, A Esfandiari, M Mohatashamifar *J. Phys. Chem. C* **114** 12955 (2010)
200. Y Qiana, S Lub, F Gaoc *Mater. Lett.* **65** 56 (2011)
201. E C Salas, Z Sun, A Lüttge, J M Tour *ACS Nano* **4** 4852 (2010)
202. W Chen, L Yan, P R Bangal *Carbon* **48** 1146 (2010)
203. Y Zhu, S Murali, M D Stoller, A Velamakanni, R D Piner, R S Ruoff *Carbon* **48** 2118 (2010)
204. V N Gorshenev *Russ. J. Phys. Chem. B* **5** 780 (2011)
205. L Cote, R Cruz-Silva, J Huang *J. Am. Chem. Soc.* **131** 1170 (2009)

206. D A Sokolov, K R Shepperd, T M Orlando *J. Phys. Chem. Lett.* **1** 2633 (2010)
207. M Baraket, S G Walton, Z Wei, E H Lock, J T Robinson, P Sheehan *Carbon* **48** 3382 (2010)
208. P Yao, P Chen, L Jiang, H Zhao, H Zhu, D Zhou, W Hu, B H Han, M Liu *Adv. Mater.* **22** 5008 (2010)
209. Z Wei, D Wang, S Kim, S Y Kim, Y Hu, M K Yakes, A R Laracuente, Z Dai, S R Marder, C Berger *Science* **328** 1373 (2010)
210. D Yang, A Velamakanni, G Bozoklu, S Park, M Stoller, R D Piner, S Stankovich, I Jung, D A Field, C A Ventrice Jr, R S Ruoff *Carbon* **47** 145 (2009)
211. Y Zhu, M D Stoller, W Cai, A Velamakanni, R D Piner, D Chen, R S Ruoff *ACS Nano* **4** 1227 (2010)
212. D Wei, Y Liu, Y Wang, H Zhang, L Huang, G Yu *Nano Lett.* **9** 666 (2009)
213. N Lia, Z Wang, K Zhao, Z Shi, Z Gu, S Xu *Carbon* **48** 255 (2010)
214. L S Panchakarla, K S Subrahmanyam, S K Saha, A Govindaraj, H R Krishnamurthy, U V Waghmare, C N R Rao *Adv. Mater.* **21** 4726 (2009)
215. C T Hach, L E Jones, C Crossland, P A Throver *Carbon* **37** 221 (1999)
216. M Endo, T Hayashi, S H Hong, T Enoki, M S Dresselhaus *J. Appl. Phys.* **90** 5670 (2001)
217. K Yuge *Phys. Rev. B* **79** 144109 (2009)
218. L Ci, L Song, C Jin, D Jariwala, D Wu, Y Li, A Srivastava, Z F Wang, K Storr, L Balicas, F Liu, P M Ajayan *Nat. Mater.* **9** 430 (2010)
219. Y Gao, Y Zhang, P Chen, Y Li, M Liu, T Gao, D Ma, Y Chen, Z Cheng, X Qiu, W Duan, Z Liu *Nano Lett.* **13** 3439 (2013)
220. E G Gal'pern, V V Pinyaskin, I V Stankevich, L A Chernozatonskii *J. Phys. Chem. B* **101** 705 (1997)
221. L A Chernozatonskii, E G Gal'pern, I V Stankevich, Y K Shimkus *Carbon* **37** 117 (1999)
222. S Bhowmick, A K Singh, B I Yakobson *J. Phys. Chem. C* **115** 9889 (2011)
223. Y Ding, Y Wang, J Ni *Appl. Phys. Lett.* **95** 123105 (2009)
224. L Song, L Ci, H Lu, P B Sorokin, C Jin, J Ni, A G Kvashnin, D G Kvashnin, J Lou, B I Yakobson, P M Ajayan *Nano Lett.* **10** 3209 (2010)
225. P Sutter, R Cortes, J Lahiri, E Sutter *Nano Lett.* **12** 4869 (2012)
226. M P Levendorf, C J Kim, L Brown, P Y Huang, R W Havener, D A Muller, J Park *Nature (London)* **488** 627 (2012)
227. I I Naumov, A M Bratkovsky *Phys. Rev. B* **84** 245444 (2011)
228. J Hicks, A Tejada, A Taleb-Ibrahimi, M Nevius, F Wang, K Shepperd, J Palmer, F Bertran, P Le Fèvre, J Kunc, W A de Heer, C Berger, E H Conrad *Nat. Phys.* **9** 49 (2013)
229. L A Chernozatonskii, P B Sorokin, A G Kvashnin, D G Kvashnin *J. Exp. Theor. Phys. Lett.* **90** 134 (2009) [*Pis'ma Zh. Eksp. Teor. Fiz.* **90** 144 (2009)]
230. V N Mitkin *J. Struct. Chem.* **44** 82 (2003) [*Zh. Strukt. Khim.* **44** 99 (2003)]
231. L A Chernozatonskii, P B Sorokin, A A Kuzubov, B P Sorokin, A G Kvashnin, D G Kvashnin, P V Avramov, B I Yakobson *J. Phys. Chem. C* **115** 132 (2011)
232. D K Samarakoon, X Q Wang *ACS Nano* **4** 4126 (2010)
233. H J McSkimin, P Andreatch *J. Appl. Phys.* **43** 2944 (1972)
234. O Leenaerts, B Partoens, F M Peeters *Phys. Rev. B* **80** 245422 (2009)
235. L Zhu, H Hu, Q Chen, S Wang, J Wang, F Ding *Nanotechnology* **22** 185202 (2011)
236. L A Chernozatonskii, B N Mavrin, P B Sorokin *Phys. Status Solidi, B* **249** 1550 (2012)
237. A C Ferrari, J C Meyer, V Scardaci, C Casiraghi, M Lazzeri, F Mauri, S Piscanec, D Jiang, K S Novoselov, S Roth, A K Geim *Phys. Rev. Lett.* **97** 187401 (2006)
238. C Cong, T Yu, K Sato, J Shang, R Saito, G F Dresselhaus, M S Dresselhaus *ACS Nano* **5** 8760 (2011)
239. R Ruoff *Nature (London)* **483** S42 (2012)
240. A B Dalton, S Collins, E Musoz, J M Razal, V H Ebron, J P Ferraris, J N Coleman, B G Kim, R H Baughman *Nature (London)* **423** 703 (2003)
241. S Stankovich, D A Dikin, G H B Dommett, K M Kohlhaas, E J Zimney, E A Stach, R D Piner, S T Nguyen, R S Ruoff *Nature (London)* **442** 282 (2006)
242. S Watcharotone, D A Dikin, S Stankovich, R Piner, I Jung, G H B Dommett, G Evmenenko, S E Wu, S F Chen, C P Liu, S T Nguyen, R S Ruoff *Nano Lett.* **7** 1888 (2007)
243. D Cai, M Song, C Xu *Adv. Mater.* **20** 1706 (2008)
244. C C Chen, C F Chen, I H Lee, C L Lin *Diamond Relat. Mater.* **14** 1897 (2005)
245. D Kondo, S Sato, Y Awano *Appl. Phys. Exp.* **1** 074003 (2008)
246. E F Sheka, L A Chernozatonskii *J. Comput. Theor. Nanosci.* **7** 1814 (2010)
247. C Li, Z Li, H Zhu, K Wang, J Wei, X Li, P Sun, H Zhang, D Wu *J. Phys. Chem. C* **114** 14008 (2010)
248. Y K Kim, D H Min *Langmuir* **25** 11302 (2009)
249. D H Lee, J E Kim, T H Han, J W Hwang, S Jeon, S Y Choi, S H Hong, W J Lee, R S Ruoff, S O Kim *Adv. Mater.* **22** 1247 (2010)
250. C L Pint, N T Alvarez, R H Hauge *Nano Res.* **2** 526 (2009)
251. Z Yan, L Ma, Y Zhu, I Lahiri, M G Hahn, Z Liu, S Yang, C Xiang, W Lu, Z Peng, Z Sun, C Kittrell, J Lou, W Choi, P M Ajayan, J M Tour *ACS Nano* **7** 58 (2012)
252. T Saito, H Chiba, T Ito, T Ogino *Carbon* **48** 1305 (2010)
253. Q Su, Y Liang, X Feng, K Müllen *Chem. Commun.* **46** 8279 (2010)
254. D Yu, L Dai *J. Phys. Chem. Lett.* **1** 467 (2009)
255. U Khan, I O'Connor, Y K Gun'ko, J N Coleman *Carbon* **48** 2825 (2010)
256. R Lv, T Cui, M S Jun, Q Zhang, A Cao, D S Su, Z Zhang, S H Yoon, J Miyawaki, I Mochida, F Kang *Adv. Funct. Mater.* **21** 999 (2011)
257. L A Chernozatonskii, E F Sheka, A A Artyukh *J. Exp. Theor. Phys. Lett.* **89** 352 (2009) [*Pis'ma Zh. Eksp. Teor. Fiz.* **89** 412 (2009)]
258. L A Chernozatonskii, P B Sorokin *ECS Transact.* **19** 35 (2009)
259. A A Artyukh, L A Chernozatonskii, P B Sorokin *Phys. Status Solidi, B* **247** 2927 (2010)
260. Y Li, F Sun, H Li *J. Phys. Chem. C* **115** 18459 (2011)
261. D Xia, Q Xue, J Xie, H Chen, C Lv, F Besenbacher, M Dong *Small* **6** 2010 (2010)
262. I V Lebedeva, A M Popov, A A Knizhnik, A N Khlobystov, B V Potapkin *Nanoscale* **4** 4522 (2012)
263. Y H Ho, Y H Chiu, J M Lu, M F Lin *Physica E* **42** 744 (2010)
264. V V Ivanovskaya, A Zobelli, P Wagner, M I Heggie, P R Briddon, M J Rayson, C P Ewels *Phys. Rev. Lett.* **107** 065502 (2011)
265. M A Akhukov, S Yuan, A Fasolino, M I Katsnelson *New J. Phys.* **14** 123012 (2012)

266. V Jousseume, J Cuzzocrea, N Bernier, V T Renard *Appl. Phys. Lett.* **98** 123103 (2011)
267. X Lu, H Dou, B Gao, C Yuan, S Yang, L Hao, L Shen, X Zhang *Electrochim. Acta* **56** 5115 (2011)
268. J Yan, T Wei, Z Fan, W Qian, M Zhang, X Shen, F Wei *J. Power Sources* **195** 3041 (2010)
269. Z Fan, J Yan, L Zhi, Q Zhang, T Wei, J Feng, M Zhang, W Qian, F Wei *Adv. Mater.* **22** 3723 (2010)
270. P Chen, X Wu, J Lin, K L Tan *Science* **285** 91 (1999)
271. C Ataca, E Aktmrk, S Ciraci, H Ustunel *Appl. Phys. Lett.* **93** 043123 (2008)
272. C Ataca, E Aktmrk, S Ciraci *Phys. Rev. B* **79** 41406 (2009)
273. H Lee, J Ihm, M L Cohen, S G Louie *Nano Lett.* **10** 793 (2010)
274. L Y Antipina, P V Avramov, S Sakai, H Naramoto, M Ohtomo, S Entani, Y Matsumoto, P B Sorokin *Phys. Rev. B* **86** 085435 (2012)
275. G J Kubas *J. Organomet. Chem.* **635** 37 (2001)
276. S Bhattacharya, A Bhattacharya, G P Das *J. Phys. Chem. C* **116** 3840 (2011)
277. H Q Zhu, Y M Zhang, L Yue, W S Li, G L Li, D Shu, H Y Chen *J. Power Sources* **184** 637 (2008)
278. M P Ramuz, M Vosgueritchian, P Wei, C Wang, Y Gao, Y Wu, Y Chen, Z Bao *ACS Nano* **6** 10384 (2012)
279. Z Wang, J Wang, Z Li, P Gong, X Liu, L Zhang, J Ren, H Wang, S Yang *Carbon* **50** 5403 (2012)
280. Z-D Huang, B Zhang, S-W Oh, Q-B Zheng, X-Y Lin, N Yousefi, J-K Kim *J. Mater. Chem.* **22** 3591 (2012)
281. A Mathkar, T N Narayanan, L B Alemany, P Cox, P Nguyen, G Gao, P Chang, R Romero-Aburto, S A Mani, P M Ajayan *Part. Part. Syst. Character.* **30** 266 (2013)
282. I Meric, M Y Han, A F Young, B Ozyilmaz, P Kim, K L Shepard *Nat. Nanotechnol.* **3** 654 (2008)
283. *Prospects of Graphene Transistors for High-frequency Electronics – Printed Electronics World.* <http://www.printedelectronicsworld.com/articles/prospects-of-graphene-transistors-for-high-frequency-electronics-00005226.asp>
284. J Zheng, L Wang, R Quhe, Q Liu, H Li, D Yu, W-N Mei, J Shi, Z Gao, J Lu *Sci. Rep.*, **3** 1314 (2013)
285. W Lu, P Soukiassian, J Boeckl *MRS Bull.* **37** 1119 (2012)
286. M Xu, L Tao, S Minmin, H Chen *Chem. Rev.* **113** 3766 (2013)